AD-A160 291 DIELECTRIC ANALYSIS OF THERMOSET CURE(U) MASSACHUSETTS INST OF TECH CAMBRIDGE CENTER FOR MATERIALS SCIENCE AND ENGINEERING S D SENTURIA ET AL. 07 OCT 85 1/1

UNCLASSIFIED N00014-84-K-0274 F/G 11/9 NL

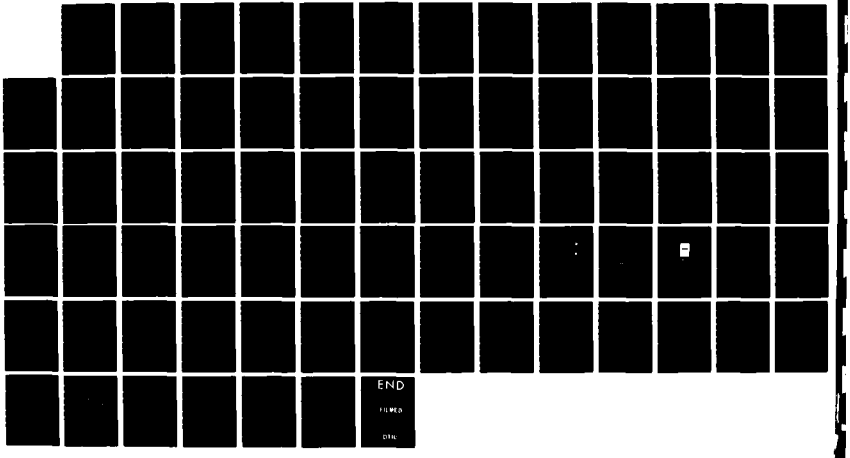

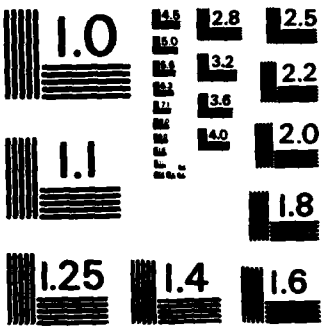

MICROCOPY RESOLUTION TEST CHART
NATIONAL BUREAU OF STANDARDS - 1963 - A

OFFICE OF NAVAL RESEARCH

Contract N00014-84-K-0274

Task No. NR 039-260

TECHNICAL REPORT NO. 4

DIELECTRIC ANALYSIS OF THERMOSET CURE

by

Stephen D. Senturia and Norman F. Sheppard, Jr.

Review Article prepared for publication in

Advances in Polymer Science

MASSACHUSETTS INSTITUTE OF TECHNOLOGY
Department of Electrical Engineering and Computer Science, and
Center for Materials Science and Engineering
Cambridge MA 02139

October 7, 1985

UNCLASSIFIED

SECURITY CLASSIFICATION OF THIS PAGE (When Data Entered)

REPORT DOCUMENTATION PAGE		READ INSTRUCTIONS BEFORE COMPLETING FORM
1. REPORT NUMBER	2. GOVT ACCESSION NO. AD-A160	3. RECIPIENT'S CATALOG NUMBER 291
4. TITLE (and Subtitle) Dielectric Analysis of Thermoset Cure		5. TYPE OF REPORT & PERIOD COVERED Technical Report 5/1/84 - 10/7/85
		6. PERFORMING ORG. REPORT NUMBER Technical Report No. 4
7. AUTHOR(s) Stephen D. Senturia and Norman F. Sheppard, Jr.		8. CONTRACT OR GRANT NUMBER(s) N00014-84-K-0274
9. PERFORMING ORGANIZATION NAME AND ADDRESS Massachusetts Institute of TEchnology 77 Massachusetts Avenue Cambridge MA 02139		10. PROGRAM ELEMENT, PROJECT, TASK AREA & WORK UNIT NUMBERS NR 039-260
11. CONTROLLING OFFICE NAME AND ADDRESS Department of the Navy, Office of Naval Research 800 N. Quincy Street Arlington VA 22217		12. REPORT DATE October 7, 1985
		13. NUMBER OF PAGES 70
14. MONITORING AGENCY NAME & ADDRESS(if different from Controlling Office)		15. SECURITY CLASS. (of this report) UNCLASSIFIED
		15a. DECLASSIFICATION/DOWNGRADING SCHEDULE

16. DISTRIBUTION STATEMENT (of this Report)

This document has been approved for public release and sale; its distribution is unlimited

17. DISTRIBUTION STATEMENT (of the abstract entered in Block 20, if different from Report)

18. SUPPLEMENTARY NOTES

19. KEY WORDS (Continue on reverse side if necessary and identify by block number)

dielectric properties; thermosetting polymers; permittivity; loss factor; loss tangent; conductivity; resistivity; epoxy resins; polyimides; polyesters; phenolics; ionic impurities; dipole relaxation; microdielectrometry; Williams-Landel-Ferry equation; WLF equation; viscosity; cure

20. ABSTRACT (Continue on reverse side if necessary and identify by block number)

Measurements of dielectric properties have been used to monitor chemical reactions in organic materials for more than fifty years. This review addresses the application of dielectric measurements to thermosetting polymers including basic dielectric properties, the methods used to measure those properties, key experimental artifacts that must be understood by the investigator, the physical origin of those artifacts, and a survey of the current published literature with emphasis on the correlations between dielectric properties and other physical properties of the material.

DD FORM 1 JAN 73 1473 EDITION OF 1 NOV 65 IS OBSOLETE S/N 0102-014-6601

SECURITY CLASSIFICATION OF THIS PAGE (When Data Entered)

DIELECTRIC ANALYSIS OF THERMOSET CURE

Stephen D. Senturia, Professor of Electrical Engineering, Massachusetts Institute of Technology, Cambridge, MA 02139, USA,

and

Norman F. Sheppard, Jr., Research Assistant in Electrical Engineering, Massachusetts Institute of Technology, Cambridge MA 02139, USA

A. INTRODUCTION

A.1 Historical Perspective

Measurements of dielectric properties have been used to monitor chemical reactions in organic materials for more than fifty years. In 1934, Kienle and Race [1] reported the use of dielectric measurements to study polyesterification reactions. Remarkably, many of the major issues that are the subject of this review were identified in that early paper: the fact that ionic conductivity often dominates the observed dielectric properties; the equivalence between the conductivity measured with both DC and AC methods; the correlation between viscosity and conductivity early in cure; the fact that conductivity does not show an abrupt change at gelation; the possible contribution of orientable dipoles and sample heterogeneities to measured dielectric properties; and the importance of electrode polarization at low frequencies.

Between 1934 and 1958, the literature is sparse, but significant. Manegold and Petzoldt, writing in Germany in 1941 [2], cited a 1939 translation [3] of the abstract of a 1937 Russian article (which we were unable to obtain) by Lomakin and Gussewa [4] in which a correspondence was reported between the viscosity and both the electrical conductivity and index of refraction during the cure of phenol-formaldehyde resins. The Manegold and Petzoldt paper focuses on the conductivity changes during phenolic cure, examining the effects of both stoichiometry and catalyst variation. Their experiments included simultaneous temperature and conductivity measurements, permitting them to separate the intrinsic temperature dependence of the conductivity from the reaction-induced changes. They further demonstrated with the catalyst variation that the rate of change of conductivity after the onset of reaction varied with the reaction rate. Fineman and Puddington in 1947 [5,6] extended these conductivity studies to resorcinol-formaldehyde resins and to a commercial polyester, adding correlations with density measurements. Based on an observed similarity between the data for the two resins, only one of which loses water during cure, they concluded that the conductivity changes observed during cure were due to the changing molecular network, and not simply to water loss.

Since 1958, an extensive experimental literature has developed, primarily on epoxies, and, to a lesser extent, on polyesters, polyimides, phenolics, and other resins. Work in this area has been greatly stimulated by the increasing importance of thermosets as matrix resins in fiber reinforced composites, and by significant improvements in instrumentation and measurement methods.

One problem that has plagued the field has been the overwhelmingly empirical nature of the research, hampered by inadequate models with which to interpret the data. Furthermore, in only a few cases have the dielectric measurements been quantitatively coupled with measurements of other properties of interest, and often, experimental details that turn out to be important in hindsight, were inadvertently overlooked during the original

work. As a result, many well intentioned experiments have somehow failed to provide that cumulative insight into fundamental issues that must ultimately accompany the successful scientific application of a measurement method. Thus, a major goal of this article has been to present, within a single source, a unified review of basic dielectric properties, the methods used to measure those properties, key experimental artifacts that must be understood by the investigator, the physical origins of those artifacts, and a survey of the current published literature with emphasis on the correlations that can be found between the dielectric properties and other physical properties of the curing system.

A.2 Overview

All dielectric measurements involve the determination of the electrical polarization and conduction properties of a sample subjected to a time-varying electric field. Section B addresses dielectric measurement methods, the various instruments and electrodes, and their calibrations. Section C examines the microscopic mechanisms giving rise to the observed macroscopic dielectric properties, and Section D explores in detail the effects of temperature and cure on these properties. Finally, Section E contains a selected bibliography of applications of dielectric analysis to the study of thermoset cure.

B. DIELECTRIC MEASUREMENT METHODS

B.1 Admittance Measurements

Dielectric measurements are performed by placing a sample of the material to be studied between two conducting electrodes, applying a time-varying voltage between the electrodes, and measuring the resulting time-varying current (an "admittance" measurement). The applied voltage establishes an electric field in the sample. In response, the sample can become electrically polarized (the conventional "dielectric" response) and can also conduct net charge from one electrode to the other. Both dielectric polarization and conduction give rise to currents which can vary enormously during a cure.

It is useful to separate the phenomena associated with the measurement from the interpretation of those phenomena in terms of the dielectric properties of the sample. Figure 1 shows a "black-box" view of the sample, in which the details of the shape of the electrodes and the precise properties of the material between the electrodes are not known; only the external terminals of the electrodes are available. It is assumed that the "apparatus" of Fig. 1 applies a time-varying voltage v(t) between the terminals of the sample, and has the capability of determining either the time-varying current i(t), or the time-varying net charge Q(t), which is the time integral of the current. The discussion that follows deals with the current; an equivalent set of ideas based on charge is implied.

The interpretation of dielectric measurements assumes that the sample behavior can be represented by a linear, time-invariant admittance. The meaning of each of these terms is examined in turn.

Linearity, when dealing with time-varying signals in circuits that have energy-storage elements (such as capacitors, which are made from electrodes with a dielectric medium between them), is not the same as simple proportionality. A sufficient condition for linearity can be expressed in terms of the superposition property, as follows: a sample is linear if, given that $i_1(t)$ is the response to a particular waveform $v_1(t)$, and $i_2(t)$ is the response to a second waveform $v_2(t)$, then then the response to the waveform $av_1(t) + bv_2(t)$ (where a and b are constants) is $ai_1(t) + bi_2(t)$. (A small detail: all linear samples obey the superposition condition above provided that the net polarization charge before applying the voltage waveforms is zero. If a sample has residual polarization from previous experiments, even linear samples may fail to obey superposition.)

Whether or not a given sample actually is linear depends on the magnitude of the applied voltage. All dielectrics experience catastrophic breakdown at electric fields on the order of 10^6 volts/cm. Most dielectric measurements are made with applied voltages on the order of 1 volt, with electrode spacings ranging from tens of μm to several mm, resulting in electric fields well below breakdown. The dielectric portion of the response, therefore, is usually linear. The conduction portion of the response is often due to ions. At high enough applied voltages, electrochemical interactions at the electrodes can occur which can lead to

nonlinear conduction characteristics. There can also be intrinsically nonlinear conduction mechanisms within the medium at electric fields in excess of about 10^5 V/cm. Coln has recently looked carefully for nonlinearities in liquid epoxy resins prior to cure (where ion conduction is most important) and has found no significant nonlinear effects under normal measurement conditions [7]. It is reasonable to assume, therefore, that any sample used in conventional dielectric measurements can be considered linear.

Time-invariance presents a problem. Since the purpose of the measurement is to follow changes in dielectric and conducting properties of the sample, strictly speaking, the sample is usually not time-invariant. Yet, time-invariant circuit models are always used to interpret the results of the measurement. The justification for this practice is to assume that the sample properties change insignificantly during the interval required to make a single measurement. The degree to which this may or may not be true during actual cure studies has received relatively little attention to date, because only recently have there been commercial instruments available for cure studies below 10 Hz, where it might be possible to demonstrate explicit reaction-rate-dependent effects.

Dielectric measurements on curing systems are usually done with sinusoidal excitations at specific frequencies of interest. The frequency-dependent dielectric response of a linear time-invariant sample can be obtained by applying a step-change in voltage, measuring the resulting current waveform at a series of time intervals following the step, then computing the frequency-dependent dielectric properties from the Fourier transform of the current waveform [8]. The potential advantage of this approach is the use of digital signal processing methods to reduce the time needed to obtain data at ultra-low frequencies (to 10^{-4} Hz), but in practice, the duration of the step waveform must be short enough to keep the sample time-invariant throughout one measurement cycle. The total time for a measurement, in this case, is determined, first, by the length of time one must hold the voltage at some initial voltage (e.g., zero) before applying the step (to assure zero initial polarization charge), and second, by the length of time one must hold the voltage at its non-zero value to obtain enough data for the lowest frequency of interest. For typical thermoset cures, reaction rates usually limit the lowest useful frequency to about 0.1 Hz.

The admittance of a linear time-invariant sample can now be defined. In the sinusoidal steady state at angular frequency ω, both $v(t)$ and $i(t)$ are sinusoids having some phase difference ϕ (see Fig. 2).

$$v(t) = V_0 \cos(\omega t) \qquad \text{(B-1)}$$

$$i(t) = I_0 \cos(\omega t + \phi) \qquad \text{(B-2)}$$

where V_0 and I_0 are the real amplitudes of $v(t)$ and $i(t)$, respectively. These waveforms can be expressed in complex exponential notation, as follows:

$$v(t) = \mathrm{Re}\ \{Ve^{j\omega t}\} \qquad \text{(B-3)}$$

$$i(t) = \mathrm{Re}\ \{Ie^{j\omega t}\} \qquad \text{(B-4)}$$

where j is $(-1)^{1/2}$, and where V and I are the <u>complex amplitudes</u> of v(t) and i(t), respectively. When expressed in this form, V and I have the values

$$V = V_0 \qquad \text{(B-5)}$$

$$I = I_0 e^{j\phi} \qquad \text{(B-6)}$$

The ratio of I to V is defined as the <u>admittance</u> Y(ω) of the sample, and is written as frequency-dependent to emphasize its implicit dependence on the frequency-dependent properties of the medium.

$$Y(\omega) = I/V \qquad \text{(B-7)}$$

Substituting and expanding yields

$$Y(\omega) = j(I_0/V_0)\sin\phi + (I_0/V_0)\cos\phi \qquad \text{(B-8)}$$

In this equation, the magnitude of the admittance (I_0/V_0) and the phase ϕ are both frequency-dependent quantities. Nevertheless, at some particular frequency, it is possible to construct an equivalent circuit consisting of a capacitor $C_x(\omega)$ in parallel with a resistor $R_x(\omega)$, as shown in Fig. 3. (For clarity in this introductory discussion, the subscript "x" is used to denote "experimentally measured quantities" to distinguish them from bulk properties of materials, which are given without subscripts.) Until the electrode geometry is specified, the capacitor and resistor have no direct physical interpretation in terms of dielectric properties of the sample; they simply provide a convenient way of describing the results of the measurement. Electrode geometries are considered in the following section. For the parallel R_x-C_x circuit of Fig. 3, the admittance is written

$$Y(\omega) = j\omega C_x(\omega) + 1/R_x(\omega) \qquad \text{(B-9)}$$

which, by comparison with Eq. B-8, yields

$$C_x(\omega) = \frac{I_0 \sin\phi}{\omega V_0} \qquad \text{(B-10)}$$

and

$$R_x(\omega) = \frac{V_0}{I_0 \cos\phi} \qquad \text{(B-11)}$$

Another quantity also used in admittance measurements is the dissipation factor D, which is useful because it depends only on the phase of the admittance, not on its magnitude. The dissipation factor of a parallel R_x-C_x circuit is defined as

$$D = \frac{1}{\omega R_x C_x} \qquad \text{(B-12)}$$

which from Eqs. B-10 and B-11, yields

$$D = \text{cotan}\phi \qquad \text{(B-13)}$$

The final quantity to be defined has been the source of much confusion. The loss tangent of the sample is the same as the dissipation factor defined above; however, the loss tangent of the medium is a dielectric property. To distinguish between them, we shall refer to $\tan\delta_x$ as the sample loss tangent, having the value

$$\tan\delta_x = D \qquad \text{(B-14)}$$

Therefore, δ_x is $\pi/2 - \phi$. The loss tangent of the medium, which we shall refer to as $\tan\delta$ without a subscript, is discussed in Section C.

B.2 Electrode Geometries and Their Calibrations

B.2.1 Definitions

The dielectric permittivity of a medium measures the polarization of the medium per unit applied electric field. The permittivity of free space, ε_0 has the value 8.85×10^{-14} Farads/cm. Throughout this paper, we shall express the dielectric properties of a medium relative to ε_0. That is, the permittivity of a medium is written $\varepsilon'\varepsilon_0$, where ε' is the relative permittivity, also referred to as the dielectric constant of the medium (but remember that the dielectric "constant" changes with temperature and cure).

The dielectric loss factor arises from two sources: energy loss associated with the time-dependent polarization, and bulk conduction. The loss factor is written $\varepsilon''\varepsilon_0$, where ε'' is the relative loss factor.

The loss tangent of a medium, denoted by $\tan\delta$, is defined as the ratio $\varepsilon''/\varepsilon'$ (see also Section B.1 for the loss tangent of a sample, $\tan\delta_x$).

B.2.2 Parallel Plate Electrodes

Parallel plates are often used as electrodes in cure studies; their use in this application is first cited by Manegold and Petzold [2] and later by Aukward and Warfield [9]. Figure 4 illustrates parallel conductors of area A separated by spacing L. The sample medium is placed between the plates, or the plates can be fully immersed in the medium. Normally, one designs the plate spacing to be much less than the plate size, which minimizes the

effects of fringing fields and leads to a very simple calibration. After accounting for any cabling admittances (see Sec. B.3.1), the components of the equivalent circuit of Fig. 3 have the values:

$$C_x = \frac{\varepsilon'_x \varepsilon_0 A}{L} \qquad \text{(B-15)}$$

and

$$R_x = \frac{L}{\omega A \varepsilon''_x \varepsilon_0} \qquad \text{(B-16)}$$

where ε'_x and ε''_x denote the experimental values that are inferred for ε' and ε'', respectively, and where, to be consistent with the units selected for ε_0, linear dimensions are in cm.

For a homogeneous dielectric medium, in the absence of interface effects (see Sec. C.2), the experimental quantities ε'_x and ε''_x are equal to the bulk properties ε' and ε'', and the experimental loss tangent becomes

$$\tan\delta_x = \tan\delta \qquad \text{(B-17)}$$

That is, for a parallel plate structure containing a homogeneous medium and having no interface effects, the phase angle of the sample admittance determines the loss tangent of the medium, regardless of the plate spacing and area (within wide limits). Of course, if calibrated measurements of either ε' or ε'' are needed (and, as will be shown, they usually are), then it is necessary to measure and control both plate spacing and area to obtain quantitative results. The "cell constant" calibration method, in which the ratio A/L in Eq. B-15 is implicitly determined by measuring the electrode capacitance in air ($\varepsilon' = 1.0$), is not sufficient for calibration in the presence of interface effects; L must be known separately (see Section C.2).

The primary advantages of parallel plate electrodes lie in the ease with which measured data can be interpreted, and in the fact that they can be made from almost any conductor. The primary disadvantages are the need to control plate spacing and area if quantitative measures of either ε' or ε'' are to be obtained, and the instrumental difficulties associated with making admittance measurements at frequencies below about 100 Hz (see Section B.3) Furthermore, in cure experiments, matrix resins typically go through significant dimensional changes either due to temperature, to reaction-induced contraction, or to applied pressure, and it has proved difficult to maintain the calibration of parallel plates in these cases. This has led to almost complete reliance on the measured $\tan\delta_x$ in following cure, but as is shown in Section C.2, interface effects lead to complex artifacts in $\tan\delta_x$. As a result of these disadvantages, the use of parallel plates for quantitative studies is decreasing relative to the use of comb electrodes.

B.2.3 Comb Electrodes

The use of interdigitated, or comb electrodes for cure measurement was first reported by Armstrong [10]. The metal electrodes, illustrated schematically in Fig. 5a, are typically fabricated on an insulating substrate using photopatterning. The substrate can be a ceramic, a thin plastic film, a sheet of epoxy-glass composite, or even a silicon integrated circuit. The cross section in Fig. 5b illustrates the case where the insulating substrate is much thicker than the spacing between fingers. The calibration of the device is found by determining the admittance between the arrays of parallel stripe electrodes located at the interface between one medium having the ε' and ε'' values of the sample, the other medium having the ε' and ε'' values of the substrate. In general, this calibration cannot be calculated for exact device geometries without numerical methods. If the interdigitated portion of the electrodes is sufficiently large, the structure can be approximated by an infinite periodic comb structure, for which both analytical and simplified numerical calibrations can be obtained [11,12]. The cell constant calibration method fails for comb electrodes even in the absence of interface effects because of the relatively large component of fringing field in the substrate.

The advantages of comb electrodes lie in the reproducibility of the calibration (which permits separation of ε' and ε''), and in the ease with which they can be placed into a variety of structures, such as adhesive joints and fiber-reinforced laminates. The calibration depends on the electrode size and spacing and on the dielectric properties of the substrate, all of which can be made quite reproducible with photopatterning technology. Furthermore, the calibration is relatively insensitive to temperature or pressure changes, a major advantage compared with parallel plates. Finally, when combined with suitable blocking or release layers (see Sec. C.2), comb electrodes can be used in fiber-reinforced laminates containing graphite fibers, which are such good conductors that they interfere substantially with parallel plate measurements. The major disadvantage of comb electrodes is that they are much less sensitive than parallel plates of comparable dimensions. As a result, their primary application is in those materials where the loss factor is dominated by conductivity effects and where the conductivity is relatively large, i.e., greater than about 10^{-8} $(\Omega\text{-cm})^{-1}$ (see Section C.1). This class of materials is sufficiently large to provide a large domain of application for comb electrodes.

An important variation of the comb electrode approach is found in microdielectrometry [13,14]. The microdielectrometer sensor combines a comb electrode with a pair of field-effect transistors in a silicon integrated microcircuit to achieve sensitivities comparable with parallel-plate electrodes, but retaining the reproducible calibration features of the comb. The cross-section of Figure 6 shows the electrodes separated from a conducting ground plane (the silicon substrate) by a silicon dioxide insulator whose thickness is much less than the electrode spacing. One of the electrodes is driven with a signal, the other is connected to the input gate of one of the field-effect transistors, and except for a capacitance C_L between this electrode and the ground plane, is electrically floating. The

capacitance C_L integrates the current reaching the floating electrode through the comb electrode admittance $Y(\omega)$, and develops a voltage which depends on the charge rather than the current. Therefore, instead of providing a direct measurement of $Y(\omega)$, the microdielectrometer measures this voltage, or, equivalentely, the complex transfer function $H(\omega)$ defined as follows:

$$H(\omega) = \frac{Y(\omega)}{1 + j\omega C_L Y(\omega)} \qquad \text{(B-18)}$$

Like the admittance $Y(\omega)$, the transfer function $H(\omega)$ has a magnitude and phase which can be interpreted in terms of an assumed homogeneous dielectric medium with permittivity ε' and loss factor ε'' [12]. Figure 7 illustrates such a calibration as a contour plot. Given the magnitude and phase of $H(\omega)$, the corresponding ε' and ε'' values can be determined. Furthermore, as was the true for the parallel plates and simple comb electrodes, calibrations like that of Figure 7 implicitly assume a homogeneous dielectric medium and no interface effects. In practice, however, interface effects are almost always observed at the early stages of thermoset cure (see Section C.2).

A schematic of a microdielectrometer sensor is shown in Figure 8 and illustrates the electrode array, the field-effect transistors and a silicon diode temperature indicator [15] which functions as a moderate accuracy (~2 °C) thermometer between room temperature and 250 °C. The sensor is used either by placing a small sample of resin over the electrodes, or by embedding the sensor in a reaction vessel or laminate. Since all dielectric and conductivity properties are temperature dependent, the ability to make a temperature measurement at the same point as the dielectric measurement is a useful feature of this technique.

B.2.4 Other Electrodes

Many electrode patterns have been used for cure studies. Kienle and Race [1] used parallel cylindrical conductors immersed in the medium. Coaxial cylinder electrodes, with the sample placed between the two cylinders, were first used by Fineman and Puddington [5,6], and later by Aukward, Warfield, and Petree [16]. The coaxial electrodes, like the parallel plates, have a relatively simple calibration, but are tedious to construct reproducibly for each thermoset cure experiment. Generally, any electrode configuration can be used for observing trends, but electrode size and location must be reproducibily controlled if calibrated measurements are desired.

B.3 Measurement Equipment

B.3.1 Capacitance and Impedance Bridges

Whether using parallel plate or comb electrodes, the basic measurement involves determining the admittance between the electrodes under sinusoidal steady-state conditions (the lone exception is the microdielectrometer, discussed in Section B.3.2). Many early studies were made with general-purpose capacitance bridges designed for measurements of capacitors with small loss tangents. Because thermoset resins become relatively conductive when they are heated, particularly early in cure, such capacitance bridges could not be used without the addition of an insulating (or blocking) layer between at least one of the electrodes and the sample to lower the overall loss tangent of the sample to within the instrument range. However, this significantly modifies the calibration (see Section C.2).

The first commercial admittance bridge specifically directed toward resin-cure applications was introduced by Tetrahedron Associates in 1969 [17]. Within the past decade, a variety of general-purpose instruments suitable for resin-cure applications have been introduced. Examples from major U.S. manufacturers include the Hewlett-Packard HP4192A Low Frequency Impedance Analyzer [18], and the GenRad 1689 Digibridge [19]. Either can provide measurements of both R_x and C_x over a range of frequencies (11 Hz - 100 kHz for the GenRad, and 5 Hz - 13 MHz for the HP). Both are equipped with the equivalent of the standard IEEE 488 computer bus, which facilitates interfacing and control from a variety of data-logging computers or desktop calculators.

The effectiveness of these instruments for dielectric cure studies depends on sensitivity and accuracy. The sensitivity is related to the minimum resolvable phase angle, which for general cure studies, should ideally be less than about 0.1°. Unfortunately, actual sensitivity in use depends strongly on the measurement frequency, on the admittance of the sample, on the details of the cabling and shielding, and on the electrical noise level of the environment. Therefore, analysis of published sensitivity specifications is difficult. It is easier to evaluate intrinsic instrument accuracy, which can be expressed in terms of either the $\tan\delta_x$ accuracy or the conductivity accuracy. An example is useful.

A pair of 1 cm^2 area plates spaced apart by 0.25 mm and filled with a resin having a permittivity of 10 (a typical value early in cure) has a capacitance of about 35 pF. The HP4192A has a $\tan\delta_x$ accuracy of 0.002 when measuring 35 pF at 1000 Hz [18], which is satisfactory for most resin studies at that frequency. However, the $\tan\delta_x$ accuracy of the HP4192A degrades to about .05 at 5 Hz, which limits the smallest conductivity that can be measured. In the final stages of typical cures, ε' approaches a value of 4-5, while ε'' approaches a value that depends on frequency. At low frequencies, the ε'' value is usually dominated by ionic conductivity, denoted by σ (see Sec. C.1.1). In this case, the resistance R_x is $L/\sigma A$, which when combined with Eq. B-16 yields

$$\sigma = \omega\varepsilon_0\varepsilon'\tan\delta_x \qquad \text{(B-19)}$$

If at 5 Hz, $\tan\delta_x$ is only accurate to .05, and using $\varepsilon' = 4$, the corresponding accuracy for σ is 1.9×10^{-13} $(\Omega\text{-cm})^{-1}$. For many materials including epoxies, it is desirable to measure σ values into the 10^{-14} $(\Omega\text{-cm})^{-1}$ range, or lower.

Additional problems are introduced by the overall admittance level and by cabling and shielding issues. In Fig. 8, the parallel-plate sample is connected to a meter by a coaxial cable (~100 pF/meter). A 2-meter cable introduces a capacitance of 200 pF in parallel with the sample, which must be subtracted from the measured capacitance to determine the sample capacitance. Clearly, when the cable capacitance is comparable to the sample capacitance, sensitivity and accuracy are reduced. Furthermore, unless the cable and electrodes are shielded, pickup at 60 Hz and its harmonics can degrade measurements at or near those frequencies. Finally, at frequencies below 100 Hz, the magnitude of the sample admittance becomes small (~ 2×10^{-9} Ω^{-1} at 100 Hz, and decreasing proportional to ω at lower frequencies), and becomes comparable to stray or leakage admittances within the instrument. In practice, it has proved difficult to operate admittance-measuring instruments below about 10 Hz, and even an instrument with an ideal $\tan\delta_x$ sensitivity as low as 0.001, if restricted by cabling problems to a useful frequency range of 10 Hz or above, cannot measure a conductivity smaller than about 1.5×10^{-14} $(\Omega\text{-cm})^{-1}$.

B.3.2 Microdielectrometry

Microdielectrometry was introduced as a research method in 1981 [14], and became commercially available in 1983 [20]. The microdielectrometry instrumentation combines the pair of field-effect on the sensor chip (see Sec. B.2.3) with external electronics to measure the transfer function $H(\omega)$ of Eq. B-18. Because the transistors on the sensor chip function as the input amplifier to the meter, cable admittance and shielding problems are greatly reduced. In addition, the use of a charge measurement rather than the admittance measurement allows the measurements to be made at arbitrarily low frequencies. As a matter of practice, reaction rates in cure studies limits the lowest useful frequency to about 0.1 Hz; however pre-cure or post-cure studies can be made to as low as 0.005 Hz. Finally, the differential connection used for the two transistors provides first-order cancellation of the effects of temperature and pressure on the transistor operation. The devices can be used for cure measurements to 300 °C, and at pressures to 200 psi.

As described in Section B.2.3, the microdielectrometer calibration [12] is similar to that of comb electrodes. Based on the accuracy of the amplitude and phase measurement electronics, the ε'' sensitivity of the microdielectrometer is about 0.01 [7], which for a medium having a dielectric permittivity of 4 corresponds to a $\tan\delta$ sensitivity of less than 0.003. At a frequency of 0.1 Hz, an ε'' sensitivity of 0.01 corresponds to a conductivity sensitivity of about 1×10^{-16} $(\Omega\text{-cm})^{-1}$. However, the accuracy of the microdielectrometry calibration at these conductivity levels has not been rigorously established.

C. MICROSCOPIC MECHANISMS

C.1 Bulk Effects

This section examines the dielelectric and conduction mechanisms in bulk materials, assuming that the medium is linear (at the applied electric field strength) and homogeneous. Effects of interfaces and inhomogeneities are discussed in Section C.2. Additional discussion can be found in basic texts [21-23].

Two bulk effects are considered in the following Sections: ionic conductivity, and molecular dipole orientation. It is also necessary to introduce the so-called "infinite-frequency" dielectric polarization which provides the baseline against which to measure the other effects. The permittivity ε' is written schematically as

$$\varepsilon' = \varepsilon_\infty + \varepsilon'_d \qquad \text{(C-1)}$$

where ε_∞ is the baseline permittivity, and ε'_d is the additional permittivity attributed to dipole orientation. For the purpose of this review, ε'_d is associated with the major dipolar relaxation at the glass transition (the α-relaxation); it depends on frequency, temperature, and cure. The frequency-dependence is examined in Section C.1.2; the temperature and cure dependences are discussed in Section D.

The definition of ε_∞ depends somewhat on the temperature and/or frequency range used for the experiments. Typical dielectric studies take place at frequencies below about 1 MHz. At temperatures below the glass transition, there can still be dipolar contributions to ε' at these frequencies from limited motions of polar groups. However, at sufficiently low temperatures (and/or high frequencies), these groups lose the ability to align with an applied electric field, resulting in additional decreases in ε' (the β- and lower-temperature relaxations). This review does not address either the low-temperature properties of resins, or the details of these relaxations. Hence, such dipolar effects are lumped into ε_∞. Within the temperature range at which typical cures take place, ε_∞ is found not to depend significantly on frequency, temperature, or cure.

C.1.1 Ionic Conductivity

The importance of ionic conductivity in curing resins has been recognized since the earliest work [1,2]. In epoxies, Fava [24] proposed that sodium and chloride ions are the particular species involved, the origin of the ions being the reaction used to produce the starting materials. (The reaction of epichlorhydrin with bisphenol-A to make the diglycidyl ether of bisphenol-A (DGEBA) produces HCl as a byproduct which is subsequently neutralized with alkali [25].) Even after treatment to remove NaCl, there is residual chloride ion present in commercial DGEBA resins at concentrations typically on the order of tens of ppm [26], and corresponding concentrations of cations. These impurities actually provide a remarkably useful probe of the resin system.

If the electric field within the resin is E, the i^{th} species of ion will acquire an average drift velocity v_i. The assumed linearity of the medium implies that v_i is proportional to E. The proportionality constant is called the mobility of the ion, for which we use the symbol u_i.

$$v_i = u_i E \qquad \text{(C-2)}$$

If there are N_i ions of species i per unit volume, with a charge magnitude of q_i on the ith ion, the ionic conductivity σ can be expressed as

$$\sigma = \sum_i q_i N_i u_i \qquad \text{(C-3)}$$

The relation between the mobility of the ion and the properties of the resin can be qualitatively examined with the aid of Stoke's law for the drift of a spherical object in a viscous medium [see, for example, 27]. The mobility of a sphere of radius r_i embedded in a medium of viscosity η and subjected to a force $q_i E$ is

$$u_i = \frac{q_i}{6\pi\eta r_i} \qquad \text{(C-4)}$$

In this simple model, the mobility, and hence σ, varies as $1/\eta$; equivalently, the quantity $1/\sigma$, called the resistivity and denoted ρ, is nominally proportional to viscosity. It must be emphasized, however, that this Stoke's law approach is an oversimplification which fails completely as a curing resin approaches gelation. As discussed in detail in Section D, the ion mobility in a resin depends primarily on the mobilities of the polymer segments. At gelation, the bulk viscosity becomes infinite because of the formation of a macroscopic molecular network. However, the resistivity remains finite because polymer segments comparable in size to the ions are still mobile. Well before gelation, the resistivity and viscosity are tightly correlated because both the viscosity and ion mobility have similar dependences on polymer segment mobility.

Ionic conductivity has another important implication. The resin system acts like an electrolyte; thus, all of the electrode polarization effects that can be observed in conventional electrolytes can also be observed in resins. The effect of electrode polarization is discussed in Section C.2.

Conductivity effects give rise to a $1/\omega$ frequency dependence in ε'', as shown below

$$\varepsilon'' = \frac{\sigma}{\omega\varepsilon_0} + \varepsilon''_d \qquad \text{(C-5)}$$

where ε''_d is the contribution to ε'' from losses arising from dipolar orientation. This frequency dependence is examined further in the following Section.

C.1.2 Dipole Orientation

Figure 10 illustrates in highly schematic form the alignment of molecular dipoles in an applied electric field. The dipoles in a curing resin are embedded in a viscous medium, and are hindered by attachment to a growing network. The orientation process will require a characteristic time, called the dipole relaxation time and denoted by τ_d. During a typical cure reaction, τ_d is short early in cure, and becomes large when the resin vitrifies. Because of the hindering mechanism, there is energy loss associated with the orientation process.

The following notation is used to describe the dipolar quantities:

ε_u: The "unrelaxed" permittivity, equivalent to ε_∞

ε_r: The "relaxed" permittivity, equal to the bulk permittivity when molecular dipoles align with the electric field to the maximum extent possible at the sample temperature.

The simplest model of hindered dipole orientation is due to Debye [28], and assumes a single relaxation time for all molecular species. The Debye model, plus a term to account for ionic conductivity, leads to the following illustrative expressions for ε' and ε'':

$$\varepsilon' = \varepsilon_u + \frac{\varepsilon_r - \varepsilon_u}{1 + (\omega\tau_d)^2} \qquad \text{(C-6)}$$

and

$$\varepsilon'' = \frac{\sigma}{\omega\varepsilon_0} + \frac{(\varepsilon_r - \varepsilon_u)\omega\tau_d}{1 + (\omega\tau_d)^2} \qquad \text{(C-7)}$$

Figure 11a illustrates the frequency dependence of ε' for Eq. C-6. Note that ε' is midway between ε_u and ε_r when $\omega = 1/\tau_d$. The corresponding plots for ε'' are more complex, because one must assess the relative contributions of σ and the dipole loss. The simplest case is for $\sigma = 0$ (Fig. 11b), where the characteristic dipolar loss peak of amplitude $(\varepsilon_r - \varepsilon_u)/2$ is observed at frequency $\omega = 1/\tau_d$. For non-zero σ, however, the $1/\omega$ dependence of ε'' greatly distorts the ε'' curve from the ideal Debye peak. Log-log scales are helpful, as illustrated in Fig. 12. The $\sigma = 0$ case is replotted from Fig. 11b; also plotted are the frequency dependences of ε'' for σ/ε_0 having various values relative to $\varepsilon_r - \varepsilon_u$. As σ increases, it becomes increasingly difficult to discern the dipole loss peak. Roughly speaking, for σ/ε_0 greater than about three times ε_r, the observed ε'' is entirely dominated by σ. (Ideally, even when σ dominates the dipolar contribution to ε'', it should still be possible to observe the dipolar contribution to ε'; however, when σ is large, electrode polarization effects tend to dominate the ε' measurement as well. See Sec. C.2.1.)

A convenient way of displaying the ε' and ε'' frequency dependences is in a Cole-Cole plot [29], where ε'' is plotted against ε' with ω as a parameter. Figure 13 shows the Cole-Cole diagrams for the idealized cases illustrated in Figs. 11 and 12. Note that when $\sigma = 0$, the Cole-Cole diagram is a perfect semicircle, with endpoints at ε_u and ε_r and with a maximum ε'' value of $(\varepsilon_r - \varepsilon_u)/2$. As σ increases, however, the Cole-Cole diagram approaches a vertical line with an intercept on the ε' axis of ε_u.

In practice, the Cole-Cole diagrams observed differ from those of Fig. 13 in two ways. The first is due to electrode polarization, discussed in Section C.2.1; the second is due to the fact that in real materials, the dipolar hindering mechanisms are not characterized simply by one τ_d, but by some distribution of relaxation times. A variety of empirical expressions have been proposed to describe real dipolar behavior; those by Cole and Cole [29], Davidson and Cole [30], and Williams and Watts [31,32] are most often cited. Although these expressions are empirical, each implicitly specifies a shape for the relaxation time distribution. A parameter β, known as the distribution parameter, characterizes the breadth of the distribution. This parameter ranges from 0 to 1, and each expression reduces to the Debye single relaxation time when $\beta = 1$. The Cole-Cole expression leads to a symmetric distribution of relaxation times about the mean value. The other two expressions lead to asymmetric distributions. The Williams-Watts formula assumes a polarization decay function of the form $\exp[-(t/\tau_d)^{\beta}]$, in constrast to the a polarization decay function of the form $\exp(-t/\tau_d)$ that would result from a single relaxation time.

Figure 14 compares the Cole-Cole diagrams for a single relaxation time ($\beta = 1$), the Cole-Cole expression with $\beta = 0.5$, and the Williams-Watts expression with $\beta = 0.5$. The Cole-Cole function forms a symmetric arc, which approaches the intercepts with finite slope and has a maximum ε'' value less than $(\varepsilon_r-\varepsilon_u)/2$. The Williams-Watts function also forms a flattened arc, but is asymmetric. The shape of the Davidson-Cole function is very similar to the Williams-Watts function, as discussed by Lindsey and Patterson [33]. The evalution of the Williams-Watts function requires numerical methods [33,34]. Computer programs implementing this function from published tabular values are readily available [35].

C.2 Interface Effects

C.2.1 Electrode Polarization

The electrode-resin interface is normally electrochemically blocked at the low voltages used for dielectric measurements. This means that, just as in the case of an aqueous electrolyte, the applied electric field can polarize the electrodes by causing the accumulation of ion layers. The possibility of this effect was noted by Kienle and Race [1], and has been modeled by Johnson and Cole [36]. The first quantitative analysis of electrode polarization effects in epoxy resin cure was reported by Adamec in 1972 [37]. The implications of Adamec's work, however, which are substantial, have been largely overlooked. New attention on this problem

has resulted from the relative prominence of electrode polarization effects in low-frequency microdielectrometry data [38], but as discussed in Section C.2.2, the effect is equally important in parallel-plate studies using blocking or release layers.

Figure 15 illustrates the effect. In direct analogy to the dipole orientation example of Section C.1.2, the initially random distribution of ions becomes polarized in the electric field, with positive ions moving toward the negative electrode, and negative ions toward the positive electrode. Because the electrodes are blocking, these ions accumulate at the electrodes, producing charged layers at both electrodes. These are similar to the charge layer established by dipole orientation, but which can have a much greater charge per unit area. Thus, viewed from the electrodes, the measured sample capacitance C_x can be much greater than that produced by the dipoles. The parallel R_x-C_x circuit of Figure 3 together with the "homogenous medium" assumptions implicit in the calibration used for the measurement results in an apparent permittivity ε'_x which is much greater than the actual bulk permittivity ε'. The extent to which ε' and ε'_x differ depends on the sample inhomogeneity, as measured by the thickness of the charge layer relative to the inter-electrode distance.

To estimate the effects of electrode polarization, the equivalent circuit of Fig. 16 can be used. It shows a blocking layer capacitance C_b (actually the series combination of two identical capacitors — one at each electrode interface) together with a parallel R-C circuit representing the bulk material. The separate thicknesses of the blocking layer $2t_b$ and the total specimen length, L, must be used to construct the capacitances and resistors. The blocking layer capacitance C_b has the value

$$C_b = \frac{\varepsilon' \varepsilon_o A}{2t_b} \qquad \text{(C-8)}$$

where, for simplicity, the permittivity in the blocking layer has been assumed to be the same as in the bulk specimen.

Qualitatively, it is apparent that if the conductivity is low, hence making R large, the sample will behave as a simple dielectric with permittivity ε'. However, when the conductivity is large enough so that the admittance 1/R becomes greater than ωC, i.e., for $\tan\delta > 1$, then charging of C_b through R becomes the dominant behavior of the circuit. Under these circumstances, the relative magnitudes of R and C_b must be examined. If $\omega C_b > 1/R$, then charging of C_b (i. e., electrode polarization) is not significant. However, when $1/R > \omega C_b$, the charging of C_b becomes important. These arguments lead to two inequalities that must be satisfied if blocking layer effects are to be observed:

$$\tan\delta > 1 \qquad \text{(C-9)}$$

and

$$\tan\delta > \frac{L}{2t_b} - 1 \qquad \text{(C-10)}$$

The circuit model of Fig. 16 can be analyzed by transforming the circuit to the equivalent form of Fig. 3 and applying equations B-15 and B-16. The resulting values of ε'_x and ε''_x depend on the properties of the medium (ε', ε'', and $\tan\delta$) and on the ratio $L/2t_b$, as follows [38]:

$$\varepsilon'_x = \varepsilon' \frac{L}{2t_b} \left[\frac{(\tan\delta)^2 + \left(\frac{L}{2t_b}\right)}{(\tan\delta)^2 + \left(\frac{L}{2t_b}\right)^2} \right] \qquad \text{(C-11)}$$

$$\varepsilon''_x = \varepsilon'' \frac{L}{2t_b} \left[\frac{\left(\frac{L}{2t_b} - 1\right)}{(\tan\delta)^2 + \left(\frac{L}{2t_b}\right)^2} \right] \qquad \text{(C-12)}$$

The experimental loss tangent, $\tan\delta_x$, is obtained from $\varepsilon''_x/\varepsilon'_x$. In the ideal case of no electrode polarization ($L >> t_b$), these equations reduce to $\varepsilon'_x = \varepsilon'$, $\varepsilon''_x = \varepsilon''$, and $\tan\delta_x = \tan\delta$, as expected.

The experimental Cole-Cole diagrams in the presence of a polarization layer, even for a medium in which ε'_d is zero, resemble Debye-model semicircles. This is characteristic of systems with a single relaxation time, which in this case is the time required to charge the blocking layer through the medium. Figure 17 shows experimental data for a DGEBA resin on a microdielectrometer sensor [38] superimposed on Cole-Cole diagrams calculated from Equations C-11 and C-12. The temperature and frequency were varied to achieve a wide range of bulk ε'' values, and for two of the curves, polyimide coatings of 1500 Å and 1.2 μm were used to cover the electrodes. Similar Cole-Cole plots have been reported by Zukas, et. al., [39] in a parallel-plate epoxy-cure experiment in which a PTFE blocking film was used on one electrode. Even in the absence of these added coatings, nominally bare electrodes show blocking characteristics, with a blocking layer thickness of about 60 Å at the interface between epoxy resins and aluminum electrodes [38].

The presence of electrode polarization layers can have a profound effect on the interpretation of dielectric cure data. This is discussed in the following section.

C.2.2 Blocking and/or Release Layers

It is common practice, either to bring the sample $\tan\delta_x$ within the range of a particular instrument, or for convenience in removing electrodes from the sample, to insert a thin blocking layer or release layer between the plates of a parallel-plate capacitor, or across the surface of a comb

electrode. In both cases, the added blocking layer thickness completely changes the characteristic of the observed cure data.

In a typical ramped cure, the specimen begins with a relatively small loss factor, which initially increases as the temperature is increased due to a decrease in viscosity, but which later decreases due to the effects of cure. This has been illustrated schematically in Figure 18 [38], where the topmost curve represents the initial increase and subsequent decrease of the actual bulk tanδ for a specimen during cure. The remaining curves are the values of $\tan\delta_x$ that would be observed experimentally in the presence of either an electrode polarization layer or an added blocking/release layer for various values of the ratio $L/2t_b$. Note that even a thin release layer, for example a 25 μm (.001") layer placed between 5 mm spaced plates, results in an $L/2t_b$ ratio of 100. Examination of Fig. 18 shows that for this value of $L/2t_b$, the maximum value of tanδ actually produces a minimum in the experimental $\tan\delta_x$, and that two subsidiary maxima appear in $\tan\delta_x$.

The literature is rich in examples of this "upside-down" minimum and the secondary maxima arising from electrode polarization [40-43]. Figure 19 shows Lawless' superposition of a temperature ramp, the viscosity, and the measured $\tan\delta_x$ for the cure of an Avco 5505 epoxy resin with parallel plates in the presence of Kapton release layers [42]. The minimum viscosity corresponds to the minimum in tan δ_x, but as has been emphasized, this $\tan\delta_x$ minimum actually corresponds to the maximum intrinsic tanδ. The agreement of the tanδ maximum with the viscosity minimum is a reasonable result since the viscosity minimum occurs well before gelation, where the resistivity and viscosity are correlated. The two subsidiary maxima have been variously ascribed to "events" such as "flow" or "gelation", where in fact, they simply identify the point in the experiment at which polarization of the blocking layer becomes the dominant electrical feature of the sample.

The dependence of results on $L/2t_b$ also explains why parallel-plate experiments can have calibration and reproducibility problems if the plate spacing is not rigorously controlled during a cure. Comb electrodes, in spite of the complexity of their basic calibration, offer the distinct advantage of having a rigid and reproducible electrode geometry, which permits quantitative evaluation of blocking layer effects.

C.2.3 Fibers and Fillers

There are several possible effects of internal inhomogeneities such as fibers and fillers on the measured dielectric properties of composites. Interfacial polarization can be established at any interface between media of different conductivities, leading to semicircular Cole-Cole diagrams as discussed in Section C.2.1. The parameters of the Cole-Cole diagram depend both on the dielectric properties of the media and on their geometry. The appearance of these apparent Debye-like dielectric relaxations based on nonuniform conductivity within the sample is generally referred to as the Maxwell-Wagner effect, and is well established in the dielectrics literature [23].

For non-conducting fibers, such as glass, the matrix resin is the more conductive phase, at least early in cure, and one would expect some internal polarization effects to be visible in parallel-plate data. However, in spite of a large body of literature on glass fiber composites (see Section E), we have found no clearly documented cases of Maxwell-Wagner effects in fiber-reinforced composites. We speculate that the widespread practice of using release films may obscure the effects of internal polarizations. Another possible explanation is the difficulty of obtaining quantitative and reproducible comparisons between neat resin and matrix resin data. For example, Bidstrup, et. al., [44], using microdielectrometry, have noted a quantitative discrepancy between the dielectric properties of (1) a matrix resin measured in-situ during cure of a glass circuit-board laminate and (2) a sample of neat resin flaked from the staged prepreg and cured apart from the glass fibers. The in-situ resin showed higher conductivity, possibly attributable to additional ions from the fiber or fiber sizing; no definitive explanation has been established.

In the case of graphite fibers, the fiber itself is more conductive than the resin, which can significantly affect parallel-plate measurements. Nevertheless, Pike, et. al., in 1971 [45] reported successful dielectric monitoring of cure in graphite-epoxy and graphite-polyimide laminates using parallel-plate copper electrodes separated from the laminate by glass release cloth. Their data show the pair of maxima cited in the previous section, which may be due either to internal interfacial polarization or to electrode polarization. As with the non-conducting fibers, there has been no definitive observation of Maxwell-Wagner effects in graphite composites.

D. EFFECTS OF TEMPERATURE AND CURE

D.1 General Issues

This section addresses the effects of temperature and cure on the various microscopic mechanisms presented in Section C. Since temperature is a key variable in determining the rate of cure processes, and since all of the microscopic mechanisms are dependent directly on temperature as well as indirectly on time and temperature through the cure reaction, it will prove useful to examine, first, the temperature behavior of epoxy resins themselves (without curing agent), and, second, the corresponding behavior in systems undergoing cure. Of the various epoxy resins, most of the quantitative studies involve the diglycidyl ether of bisphenol-A (DGEBA), having the general formula

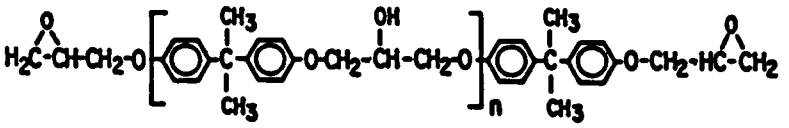

where n indicates the degree of chain extension of the resin.

Figure 20 shows the temperature dependence of the permittivity and loss factor for a DGEBA epoxy resin (EPON 828; n ≅ 0.2) in the vicinity of its glass transition (T_g = -17 °C), measured at frequencies between 0.1 and 10,000 Hz [46]. At temperatures well below T_g, the permittivity at all frequencies has a value of 4.2 (the unrelaxed permittivity), and the loss factor is below 0.1. As the temperature approaches T_g, the dipoles gain sufficient mobility to contribute to the permittivity, with evidence of this mobility increase occurring first at the lowest frequency. With a further increase in temperature, the permittivity for a given frequency levels off at the relaxed permittivity, which then decreases due to increasing temperature (see Section D.3), and then abruptly increases again as a result of electrode polarization (Section C.2). At each frequency, a dipole peak is observed in the loss factor, which then rises continuously with temperature due to an increasing ionic conductivity. The frequency at which the dipole loss peak occurs is proportional to the average dipole mobility. The ionic conductivity is proportional to the ionic mobility. Both the frequency of maximum loss and the ionic conductivity increase by many orders of magnitude over a narrow temperature range, a characteristic of relaxation processes very close to the glass transition temperature.

Figure 21 shows the permittivity and loss factor for an isothermal cure (137 °C) of DGEBA (EPON 825; n ≅ 0) with diaminodiphenylsulfone (DDS) [47]. To a first approximation, the data are the mirror image of Fig. 20, supporting the idea that the effect on electrical properties of the increase in T_g during isothermal cure might be similar to the effect of a decrease in temperature at fixed T_g. Examination of Fig. 21 shows one important difference between the temperature and cure dependences, namely that the relaxed permittivity <u>decreases</u> with cure time under isothermal conditions. This is a direct result of the changing chemistry, as discussed further in

Section D.3. The detailed behavior of the dipolar mobility is examined in Section D.4, and of the ionic mobility in Section D.5.

We shall see that throughout the literature there has been an implicit assumption of thermally activated processes, both for cure kinetics and for the intrinsic dipolar and ionic mobilities. However, it is well known that reaction kinetics become diffusion controlled at the later stages of cure, which leads to deviations from simple rate equations toward kinetics dominated by diffusive mobilities [48]. Furthermore, post-cure studies of dipolar mobilities [49-52] and studies of ion mobilities in epoxy resins [46] suggest that their temperature dependences are described by the Williams-Landel-Ferry equation [53] rather than by Arrhenius behavior. Taken together, it is fair to say that a comprehensive model of dielectric properties during a thermoset cure, including proper chemical kinetics and correct relations between state of cure, temperature, and the various dielectric parameters, has not yet been developed. However, there have been significant strides toward this goal, as the remainder of this article will demonstrate.

Two more difficulties require comment. The first is that in most of the early literature, authors did not recognize the importance of electrode polarization, and, hence, failed to make quantitative allowance for the presence of blocking and/or release layers. Thus, in most cases, it is not possible to reconstruct quantitative bulk properties from the data presented. (The present authors were not immune. They reported a correlation between a "dielectric relaxation time" and viscosity [54], failing at that time to realize that the relaxation time being studied was actually the characteristic time for electrode polarization, and, hence was dominated by conductivity.)

A second difficulty is due to an accident. In Delmonte's 1959 study of several epoxy resins [55], the time to gel and the time to vitrify were very close to one another. Delmonte identified the dipole peak as arising from the gelation event, a conclusion which has been widely cited. The incorrectness of this assignment was noted as early as 1965 by Olyphant [56], who in an excellent tutorial review of dielectric properties of curing systems, clearly identified the dipole peak with vitrification. Olyphant also stated, in agreement with the pioneering work of Warfield and Petree [57,58], that there are no electric "events" accompanying gelation. In spite of these unambiguous statements in the early literature, attempts at the electrical identification of gelation continues as a theme, aggravated by the artifacts associated with conductivity and electrode polarization. This accidental assignment of electrical signatures to gelation is discussed further in Sec. D.5.

D.2 Relation with Kinetics

In order to understand the relation between the chemical kinetics of a thermosetting system and the corresponding changes in dielectric properties, it is important to separate the various mechanisms giving rise to such changes. The relaxed permittivity is directly sensitive to the changing chemical composition, because it depends on the concentrations of the

various polar molecular segments (see Section D.3). The dipolar mobilities (Section D.4) and the ionic mobilities (Section D.5) depend on the extent of reaction primarily through the change in T_g during cure, and this dependence on T_g can be described by the WLF equation. The recognition of this WLF dependence is so recent that there have been no kinetic-dielectric studies which include it. Instead, a variety of empirical relations between dielectric properties and cure have been reported, principally in epoxy systems. These kinetic studies are reviewed in this section.

The simplest form of empirical kinetic information comes from rates of change of experimental properties, such as the time-rate-of-change of conductivity, or the cure time to reach a specific event, such as a dipole loss peak. The earliest quantitative analysis of such data was by Kienle and Race [1] who established a linear correlation between extent of esterification of alkyd resins and the corresponding log of resistivity (the resistivity, ρ, is the inverse of conductivity). Practical examples of the use of such empirical kinetic information are reviewed in Section E. Warfield and Petree [57,58], working both with diallyl phthallate and epoxy-amine resins, studied the relation between the log of resistivity and cure time at various temperatures. By identifying $d\log(\rho)/dt$ as an empirical reaction rate (an unjustified assumption; see Sec. D.5), they inferred a temperature dependence for the reaction rate, and calculated an activation energy.

The first attempt to relate changing dielectric properties to kinetic rate equations was by Kagan et. al. [59], working with a series of anyhydride-cured epoxies. Building on Warfield's assumed correlation between $d\log(\rho)/dt$ and $d\alpha/dt$, where α is the extent of epoxide conversion, they assumed a proportionality between α and $\log(\rho)$, and modeled the reaction kinetics using the equation

$$d\alpha/dt = k(1-\alpha)^m \qquad (D-1)$$

where k is the rate constant and m is the empirical reaction order. Similar analyses using mth-order kinetics have been done by Acitelli et. al. [60], working with diglycidyl ether of bisphenol-A cured with m-phenylene diamine, and by Adamec [37], working with a commercial epoxy novolac resin (Dow DEN 438) cured isothermally with 3 phr BF3-monoethylamine. Kagan extracted empirical rate constants and activation energies from his resistivity data, but did not compare these results with other methods. Acitelli used both DSC and IR data prior to gelation to compare against resistivity data obtained after the break in $\log(\rho)$ versus time (which they claim is gelation; see Sec. D.5 for a discussion). They find the same rate constant from all methods, but the empirical reaction order they must use varies enormously depending on the experimental method and on the temperature range. A similar problem in reaction order was reported by Adamec.

One difficulty with such empirical approaches based on the dielectric properties is that they tend to oversimplify the chemical kinetics, which usually are obtained from independent thermal analysis studies coupled with other measurements [61]. The epoxy-amine reaction, for example, is catalyzed by hydroxyl, hence becomes autocatalyzed as the cure proceeds

[62]. In addition, an etherification reaction can compete with the amine reaction, leading to complex branched kinetics. Sourour and Kamal [63], working with DGEBA cured with m-phenylene diamine, developed an autocatalyzed kinetic model for epoxy-amine systems using isothermal DSC measurements. Huguenin and Klein have extended the kinetic studies to the diffusion-controlled regime [48]. The use of these models to analyze the change in relaxed permittivity during the amine cure of a difunctional DGEBA epoxy is discussed in the following section.

In other chemical systems, such as tetrafunctional epoxies, polyimides, phenolics, and polyesters, there have been few attempts [64,65] to establish quantitative relationships between chemical kinetics and dielectric properties.

D.3 Relaxed Permittivity

The relaxed permittivity ε_r measures the maximum dipolar alignment that can be achieved at a given temperature and chemical state. It is observed at frequencies sufficiently low to allow dipolar alignment, but sufficiently high to avoid electrode polarization effects. In Figs. 20 and 21, the variation of ε_r with either temperature or cure must be obtained by piecing together the small intervals at each frequency where the permittivity data follow ε_r. Generally, ε_r decreases with increasing temperature, and for the case of epoxy-amine cure, decreases with increasing cure time.

The quantity ε_r is directly sensitive to the detailed chemical composition of the sample. However, the quantitative theory that relates the observed ε_r to the concentrations and dipole moments of the various polar segments present has proved quite difficult to use. The simplest approach is based on the Clausius-Mosotti equation as modified for permanent moments by Debye [28]. The Debye approach, although overly simple, revealed that ε_r should decrease with increasing temperature, and should reflect changing concentrations of polar constituents during a reaction.

The first attempt to use these ideas in epoxy cure was by Fisch and Hofmann [66], but their assignment of permittivity changes to changes in polar group concentrations was marred by what we interpret as electrode polarization effects. Blyakhman et. al. [51,52], examined the post-cure dielectric permittivity and loss tangent of anhydride-cured and amine-cured DGEBA resins. Their data are similar to that for the EPON 828 resin in Fig. 20. Based on an observed variation of the post-cure ε_r with the molecular weight of the DGEBA resin, they argue that the principal contribution to ε_r is from hydroxyether groups in the epoxy chain. Their conclusion is reasonable, since their experiments were after cure, and the highly polar curing agent and epoxides had reacted.

Huraux and co-workers, in a series of papers [67-70], and more recently, Sheppard [71], have attempted quantitative interpretation of ε_r during an epoxy cure in terms of the changing concentrations of constituent polar groups. They used a theory by Onsager which improves Debye's original theory to account for local dipole fields [see, for example, 23]. The Onsager theory, expressed below, requires some explanation:

$$\frac{(\varepsilon_r - \varepsilon_u)(2\varepsilon_r + \varepsilon_u)}{\varepsilon_r(\varepsilon_u + 2)^2} = \sum_i \frac{N_i(\mu_i)^2}{9\varepsilon_0 kT} \qquad \text{(D-2)}$$

This equation assumes that all dipoles are independent. It relates the values of ε_r and ε_u measured at temperature T to the concentrations N_i and dipole moments μ_i of the polar species (k is Boltzmann's constant and ε_0 is the permitivity of free space).

Huraux et. al., [68] used the Onsager theory to analyze the permittivity of a DGEBA resin (n=0.2) cured with a cycloaliphatic diamine. They assumed that all of the polar behavior could be attributed to epoxide groups (see below for an improved assumption), and thus extracted the time rate of change of epoxide groups from the measured rate of change of ε_r during cure using the time derivative of both sides of Eqn. D-2 (ε_u did not change either with temperature or cure). The ε_u and ε_r values were obtained by examining the Cole-Cole plots of the dipole relaxation data and extrapolating the arcs to their endpoints [67] (see Sec. D.4 for additional details). The rate of epoxy consumption was integrated to obtain the extent of conversion, which was then used to calculate an average molecular weight which was found to correlate with viscosity through a power law.

Soualmia et. al. [70] extended this approach to a specific rate equation for the chemical kinetics, which they followed independently by titration for unreacted epoxide. The system studied was a low molecular weight DGEBA resin cured with a cycloaliphatic diamine. All their measurements were at room temperature. The titration data agreed well with a second-order rate equation for the disappearance of epoxide, but in attempting to assign the reaction-dependent decrease in the dielectrically derived $\sum N_i(\mu_i)^2$ entirely to the disappearance of epoxide groups (i.e., to decreases in N_i for epoxides), they were forced to the unsatisfactory conclusion that the effective epoxide moment was changing during cure. Their dipole moment values were 5.3×10^{-30} C-m per epoxide group for the pure resin, increasing to 7.1×10^{-30} C-m when initially mixed with curing agent, and subsequently decreasing to 6.24×10^{-24} C-m at the end of cure.

One implication of Soualmia's result is that the curing agent plays a significant role in determining ε_r. This means that both the curing agent concentration and moment must be determined as part of the analysis. Sheppard [71] has attempted this for the DGEBA (n=0) system cured with DDS. Figure 22 shows ε_r versus cure time at several temperatures, obtained from data like that of Fig. 21. The extent of conversion was determined as a function of time at each temperature from independent DSC data analyzed with the autocatalyzed reaction kinetics model of Sourour and Kamal [63], which assumes that the primary and secondary amines react at the same rate, and further assumes that homopolymerization of the epoxy is negligible. This model fits the DSC data up to about 60% epoxy conversion, at which point the reaction kinetics become noticably diffusion controlled. Up to 60% conversion, however, the kinetic model can be used to calculate the concentrations of primary, secondary, and tertiary amines as functions of

time at each cure temperature. Based on the kinetic model, Sheppard extracts the temperature dependence of ε_r at constant conversion. Figure 23 shows the corresponding Onsager theory plot, i.e., the left-hand-side of Eq. D-2 plotted against 1/T. Lines extrapolated through the data points do not intersect the origin, indicating that the simple Onsager theory fails.

A similar failure of the Onsager model has been reported for polyacetaldehyde by Williams [72], and in epoxy resins by Sheppard [73]. Williams was able to analyze the polyacetaldehyde data in terms of a temperature dependent correlation between neighboring dipoles based on a conformational model of the polymer chain, and Sheppard has noted [35] that qualitatively similar conformational issues should apply to the epoxide and hydroxyl groups in the epoxy.

Both the slope and intercept point in Fig. 23 change with increasing extent of conversion, which may be due to changing N_i's and a changing interdipole correlation. To simplify the analysis, an empirical modification to the Onsager equation was used to analyze the data:

$$\frac{(\varepsilon_r - \varepsilon_u)(2\varepsilon_r + \varepsilon_u)}{\varepsilon_r(\varepsilon_u + 2)^2} = \sum_i \frac{N_i(\mu_i)^2}{9\varepsilon_0 k}\left[\frac{1}{T} - \frac{1}{T_\alpha}\right] \quad \text{(D-3)}$$

where T_α is the empirical temperature at which the plot intersects the axis for extent-of-conversion α. It is implicitly assumed that the concentrations of each polar group, N_i, depend on α based on the chemical kinetics. The data in Fig. 23 were analyzed using this model assuming three polar groups, unreacted epoxide, primary amines, and reacted amines (both secondary and tertiary). Except for the dipole moments for each species, μ_i, all quantities in Eq. D-3 were known up to 60% conversion. A fit to the data yielded the agreement shown as the solid lines in Fig. 22 using a dipole moment of 7.6×10^{-30} C-m for the epoxide, 14.8×10^{-30} for the primary amine, and 12.6×10^{-30} for the reacted amine. The larger moment values for the amine constituents demonstrate the significant contribution they make to the total ε_r value.

The work of Huraux, Soualmia, and Sheppard has demonstrated that it is possible to make a quantitative interpretation of the ε_r values (within the limits of an admittedly difficult theory), and that the ε_r value is directly linked to the chemical changes during cure. However, because of the complications introduced by dipole correlations, the relaxed permittivity is not a useful tool for routine quantitative determination of polar reactive group concentrations during cure.

D.4 Dipolar Relaxations

This section addresses the effects of temperature and cure on the dominant dipolar relaxation, i.e., the α-transition between the unrelaxed and relaxed permittivity, with its associated loss-factor peak. As illustrated in Figs. 20 and 21, this dipolar relaxation is observed as the

temperature increases through T_g, or during a cure, as T_g increases toward and even through the cure temperature.

Discussion of the dipolar relaxation involves two issues: first, the average dipolar mobility at a given temperature and degree of conversion, as measured by the frequency of the maximum in the loss factor f_{max} (or by its reciprocal, the typical dipolar relaxation time τ_d), and, second, the detailed distribution of relaxation times as measured by the frequency dependence of the permittivity and loss factor. In spite of the clear evidence that the dipolar relaxation is associated with the glass transition [56], i.e. with vitrification of a curing resin, there is also evidence that early in cure, the dipolar relaxation time correlates with viscosity [67-70,74,75]. Because the viscosity becomes infinite at gelation, it is almost "natural" (yet incorrect) to assign the dipolar relaxation to gelation [55]. The conflict in the literature can be resolved by examining the fundamental role that polymer chain mobility plays in both the viscosity and dipolar mobility.

It is helpful to begin the discussion with dipolar relaxations in pure epoxy resins, where the complexity of the gelation-vitrification issue is absent. The WLF equation [53], which is widely used to model the temperature dependence of mobility-related material properties, has the form

$$\log (a_T) = \pm \frac{C_1(T - T_S)}{C_2 + T - T_S} \qquad (D-4)$$

where the shift factor a_T is defined as the ratio of the property of interest at temperature T to the same property at a reference temperature T_S (taken as T_g in the present discussion), and where the sign of the right-hand-side is chosen according to the sign of the temperature dependence of the property being analyzed. C_1 and C_2 are constants, initially speculated as having universal values, but actually depending on the material system and on the property being measured. The important point is the dependence of the shift factor on the difference $T-T_S$.

Sheppard [46] has measured the temperature dependence of f_{max} for a homologous series of DGEBA epoxy resins with n ranging from 0 to 12. The results are plotted in Arrhenius form in Fig. 24. While it is tempting to assign activation energies to these data, careful analysis shows that there is curvature in the data, and that the results are better described by the WLF equation. The solid curves in Fig. 24 are Sheppard's WLF fit to the data, which yielded constants C_1 and C_2 that are comparable to the "universal" C_1 and C_2 values. However, the C_1 constant for the high molecular weight resins (n>2) was 50% of the value for the low MW samples (n=0, 0.2). The C_2 value decreased only slightly with n, and had a mean value of 54 °C. The C_1 decrease was attributed to the increasing dipolar contribution of hydroxyether moieties in the higher molecular weight resins, and to the speculation that these require less free volume to relax than the polar epoxide endgroups.

To connect these results to the dielectric relaxation in curing sys-

tems, it is useful to examine the post-cure data of Shito et. al. [49,50] and of Blyakhman et. al. [51,52]. Figure 25 shows the fit of Shito's data for τ_d (the reciprocal of f_{max}) to the WLF equation for a series of DGEBA resins cured with a variety of anhydrides [50]. In this case, the data were fit to the universal WLF equation, using the reference temperature as an adjustable parameter, which fell in the range 55 - 61 °C above T_g for the various samples.

The epoxy resin data and the post-cure data, taken together, show that the dipolar relaxation is associated with the temperature dependence of the polymer chain mobility in the vicinity of the glass transition. The WLF analysis of the dipolar relaxation during cure has not been carried out. In order to complete the analysis, correlated measurements of T_g, extent of cure, and dielectric properties must be made as functions of cure time and temperature. In the absence of such definitive studies, various indirect methods have been employed to analyze dielectric relaxations in curing systems, as described below.

The first method has been to draw on an expected correlation between the relaxation time and viscosity (prior to gelation). The correlation derives from elementary considerations of viscous drag on dipoles, and was originally predicted by Debye [28]. Hureux and co-workers were the first to report quantiative correlations between the mean dipole relaxation time and viscosity during epoxy cure [67-70]. Lane, et. al., have also reported such a correlation [74,75]. Furthermore, the viscosity has recently been analyzed from a WLF point of view. Tajima and Crozier [76], and Apicella, et. al., [77] have demonstrated that the temperature dependence of the viscosity during an epoxy cure can be described by a WLF equation with a reference temperature that increases with increasing extent of conversion.

The implication of all these results is a prediction that the temperature dependence of the dipole relaxation time at fixed conversion will obey the WLF equation and that the reference temperature will track the glass transition as it increases during cure. Work on this is currently under way at several laboratories.

A second method for analyzing the dipolar relaxation in curing systems is to compare isothermal cure time required to reach the dipole loss peak with cure time required to reach other events, such as vitrification as measured with torsional braid analysis. One interesting result of Sheppard's analysis of pure epoxies [46] is that the loss peak measured in the frequency range 1-3 Hz tracks T_g as measured by DSC. Extrapolating from this result, one expects that during cure the time to reach the dipole loss peak at about 1 Hz should fall near the vitrification boundary of the time-temperature-transformation (TTT) diagram [78]. In most curing systems, however, the low frequency dipole loss peaks at typical cure temperatures are obscured by the conductivity; as a result, the dipole peak is observable only at higher frequencies. Nevertheless, both the present authors [47] and Zukas, et. al. [79] have found that the temperature dependence of the time to reach the dipole peak agrees with the temperature dependence of the time to reach vitrification. Figure 26 illustrates the loss-peak data at two frequencies for EPON 825 cured with DDS superimposed on the TTT diagram

measured by Enns and Gillham using torsional braid analysis [47]. While the parallel trend with cure temperature is clear, the absolute time to reach the dipole peak at higher frequencies is systematically shorter than the time to reach vitrification.

We now examine briefly the distribution of relaxtion times. The most direct evidence for a distribution of relaxation times is the departure of the Cole-Cole plot from a perfect semicircle, as illustrated in Fig. 14. Whether one uses a Cole-Cole [29], Davidson-Cole [30] or a Williams-Watts [31,32] function to describe this distribution, a decrease in the parameter β to less than unity indicates a distribution of relaxation times. As early as 1965, Olyphant [56] noted that β was less than unity, and decreased during the cure of an anhydride-cured epoxy, indicating a broader distribution of relaxation times after cure. Huraux and co-workers [67, 70] similarly report a broadening of relaxation time distrubtion during cure. Sheppard [35] has observed a considerable decrease in the Williams-Watts β with increasing molecular weight of DGEBA resins, and also during the cure of EPON 825 with DDS. Daly and Pethrick [80] examined the relaxation data for rubber-modified epoxies, and found that β was sensitive to the rubber content of the resin.

The relation between the changing relaxation time distribution and the molecular structure of the curing system has not been determined. There is, however, one important experimental implication to these observations. Because both ε_r and β change during cure, one must actually measure the complete frequency dependence of the ε' and ε'' at a given state of cure in order to characterize the relaxation time distribution. Measurements made at one frequency throughout the cure process, when plotted on a Cole-Cole diagram, do not necessarily provide information about the relaxation time distribution.

D.5 Conductivity

This section addresses the effects of temperature and cure on the ionic conductivity. The starting point is the assumption that the ions involved are primarily impurities, such as residual sodium and chloride ions, and that their concentrations do not change appreciably during cure. This appears to be a good assumption for epoxy resins [24]. It permits conductivity changes to be interpreted in terms of changes in ion mobility, which can, in turn, be related to the mobility of the polymer chains. However, these assumptions can be expected to fail when water is a product of the curing reaction, such as in phenolic resins and some polyimides (in which a protonic conduction mechanism has been suggested [81]). If the mobile ion content is changing, analysis of the conductivity requires knowing the concentration and mobility of each mobile species, introducing complexity analogous to that encountered in Sec. D.3 in interpreting the relaxed permittivity.

As noted in Sec. C.1, resistivity and viscosity are correlated prior to gelation, a result that has been evident since the earliest work in this field [1-4,42,43,82-85]. However, as gelation is approached, the viscosity diverges, while the resistivity remains finite and varies continuously as

cure proceeds. Figure 27 illustrates this behavior with data from Tajima and Crozier [83]. In Sec. D.4, it was shown that the dipolar mobility tracks the polymer mobility through a WLF dependence on T and T_g. Similarly, one might expect that the conductivity (the reciprocal of resistivity) also tracks polymer mobility through a WLF equation. The correlation between resistivity and viscosity prior to gelation, where the viscosity obeys a WLF equation, supports this idea. Further direct evidence for the WLF behavior of the conductivity is reviewed below.

Sheppard [46] has studied the temperature dependence of the conductivity in a homologous series of DBEGA resins with n in the range from 0 to 12. The data are shown plotted in Arrhenius fashion in Fig. 28, with the solid lines representing the fit of the WLF equation to the data. Similar temperature dependences of the conductivity have been reported in fully-cured epoxy systems [24,86]. In both cases, and just as with the dipolar mobility, the driving force behind the observed temperature dependence is the mobility of the polymer as determined by the difference $T-T_g$. There are, however, differences in detail between the temperature dependences of the dipolar mobility and the conductivity. The first is that the C_1 constant Sheppard obtained for the conductivity is completely independent of the molecular weight of the resin, which suggests that the free volume required for ion transport does not depend on the structural details of the molecular matrix. A further result is that unlike the dipolar mobility, for which the C_2 constant was nearly independent of n, the C_2 constant appropriate to the conductivity tracked T_g; that is, T_g-C_2 is nearly constant.

These results can be used as a guide to interpreting conductivity data during cure using the WLF equation. As with the dipolar mobility, one would expect the temperature dependence of the conductivity at fixed conversion to obey the WLF equation and the reference temperature to track the glass transition temperature as it increases during cure. Correlated measurements of conductivity, chemical conversion, and T_g have not been reported to verify this prediction, but experiments along these lines are under way at several laboratories.

Even in the absence of direct confirming evidence, we can use the WLF approach to explain a number of results already in the literature. Figure 29 illustrates schematically how the conductivity would vary with 1/T at two different extents of chemical conversion. The arrow indicates the pathway during an isothermal cure, in which the material starts at higher conductivity, where the slope against 1/T is relatively low, and moves toward lower conductivity, where the slope is larger. The slope represents the effective "activation energy" for conductivity which would be extracted from an Arrhenius plot of conductivity over a limited temperature range. The graph shows that this apparent activation energy would increase during cure, a result first reported by Warfield and Petree in 1959 [57], and subsequently analyzed by Sheppard [35]. Conceptually, as T_g increases during cure toward the cure temperature, one is moving down the WLF curve to lower conductivity and steeper slope, hence, higher apparent activation energy.

This same idea helps explain the "knee" in the conductivity-versus-time data noted by many workers, but specifically interpreted as gelation by

Acitelli, et. al. [60]. The data are shown in Fig. 30a, including Acitelli's observation of the coincidence between the time to reach gelation and the time at which the extrapolated linear regions intersect. We now understand this coincidence; it is not related to gelation, but results from the autocatalyzed reaction kinetics coupled with the specific properties of the WLF equation, as explained below.

When time rather than temperature is the variable, the reaction kinetics must be considered. As noted earlier, the epoxy-amine cure is autocatalyzed, and consequently, the maximum rate of reaction occurs at about 30 to 40% conversion. Therefore, the time rate of change of T_g also reaches a maximum at these conversions, as demonstrated by Huguenin and Klein [48]. Furthermore, as cure proceeds, the difference $T-T_g$ decreases, and the conductivity becomes more sensitive to changes in T_g, as illustrated in Fig. 29.

The combined effect of these two mechanisms will lead to three regions of conductivity behavior in an isothermal cure. Early in cure, where the reaction rate is low and the sensitivity to T_g changes is small, the conductivity decreases relatively slowly with cure time. Later in cure, both the reaction rate and rate of change of T_g with time reach maximum values, while the sensitivity to T_g changes increases, leading to a rapidly changing conductivity with time. Finally, towards the end of cure, the reaction becomes diffusion controlled, so the change in T_g with time is very small, and the the conductivity versus time curve levels out. These three regions are clearly evident in the data of Fig. 30a. We have simulated the first two of these regions [35] by first estimating the variation of T_g with time and then obtaining the conductivity from the WLF equation using Sheppard's C_1 and C_2 constants for DGEBA resins [46]. The T_g variation was determined by combining the autocatalyzed kinetics [61, 63] with an empirical relation between T_g and α proposed by DiBennedetto, and applied to epoxy systems by Adabbo and Williams [87] and by Enns and Gillham [78]. The resulting conductivity versus time is plotted in Fig. 30b, which shows the knee of the Acitelli data at the appropriate time. Since the model used for the simulation makes no reference to gelation, we assert that the coincidence of the knee with the gel time is fortuitous. This model also shows why it is inappropriate to attempt to equate time rates of change of dielectric parameters, such as conductivity, directly to time rates of change of chemical conversion (see also Sec. D.2).

Blocking-layer effects are also sensitive to the conductivity change during cure. As demonstrated in Sec. C.2, electrode polarization can lead to a Cole-Cole diagram that is similar to the Debye equation for dipole orientation, but with much larger apparent permittivities. If the thickness of the blocking layer does not vary during cure (which will be the case if the ion content remains fixed), the "relaxation time" associated with this polarization is proportional to the resistivity of the medium, and, hence, should track viscosity early in cure. The present authors reported such a correlation [54]; Zukas, et. al., [79] have subsequently confirmed that the time to the loss peak associated with electrode polarization tracks the "isoviscous" event in torsional braid analysis.

Finally, from a pragmatic point of view, the conductivity is a very sensitive probe of cure. Not only does it become increasingly sensitive to changes in T_g as the end of cure is reached, but it can almost always be measured, even in the presence of dipolar effects, by decreasing the measurement frequency. The conductivity is equally sensitive to small decreases in T_g that result from degradation, a result first noted by Warfield [58]. Applications of conductivity measurement to cure studies are reviewed in Sec. E.

E. APPLICATIONS

In Section D, we have examined, from a fundamental point of view, how temperature and cure affect the dielectric properties of thermosetting resins. The principal conclusions of that study were (1) that conductivity (or its reciprocal, resistivity) is perhaps the most useful overall probe of cure state, (2) that dipolar relaations are associated with the glass transition (i.e., with vitrificatiton), (3) that correlations between viscosity and both resistivity and dipole relaxation time are expected early in cure, but will disappear as gelation is approached, and (4) that the relaxed permittivity follows chemical changes during cure but is cumbersome to use quantitatively.

This section presents a cross-referenced bibliography on the application of dielectric property measurements to thermosetting materials. Our literature search identified almost 200 papers with some relevance to the subject. Of these, we have selected about 70 for inclusion in this section. These papers provide particularly useful application examples, or provide data typical of the particular material or application which future investigators can use for comparisons with their own results.

The bibliography is presented in the form of two Tables. Table I references the papers by the material system under study; Table II references the papers by the application involved and/or by the type of data presented. As is evident in Table I, most of the literature involves epoxies, and most of the applications to composites are either for epoxy-glass or epoxy-graphite systems.

In the Applications categories of Table II, except for those papers identified as presenting post-cure results, all of the papers involve curing. No differentiation was made as to isothermal or ramped cure, since both types of data would be of importance to any particular resin system. The heading "Cure Rate and/or Catalyst Studies" includes those papers in which explicit correlations between cure temperature or catalyst concentration are presented, whereas the heading "General Process Monitoring" includes papers where, for the most part, commercial resin or prepreg systems are carried through nominal cure cycles.

The Data Type categories of Table II are used to identify those papers either where quantitative results on the indicated dielectric property have been obtained, or where the data is typical of the system of interest.

ACKNOWLEDGEMENT

The authors wish to acknowledge the research support of the United States Office of Naval Research during the preparation of this review, and the literature search assistance of Rebecca Miller, who received partial support through the MIT Undergraduate Research Opportunities Program.

NOMENCLATURE

α	extent of conversion
β	distribution parameter
$\tan\delta$	bulk material loss tangent
$\tan\delta_x$	experimental loss tangent (equivalent to D)
ε_0	permittivity of free space, 8.85×10^{-14} F/cm
ε_r	relaxed permittivity (relative to ε_0)
ε_u	unrelaxed permittivity (relative to ε_0; equivalent to ε'_∞)
ε'	bulk permittivity (relative to ε_0)
ε'_x	experimental permittivity (relative to ε_0)
ε'_d	dipole contribution to the relative permittivity
ε_∞	infinite-frequency relative permittivity (equivalent to ε_u)
ε''	bulk loss factor (relative to ε_0)
ε''_x	experimental loss factor (relative to ε_0)
η	viscosity
μ	dipole moment
ρ	resistivity (equivalent to $1/\sigma$)
σ	conductivity (equivalent to $1/\rho$)
τ_d	dipole relaxation time
ϕ	phase difference between voltage and current
ω	angular frequency
Ω	ohms

A	area of parallel plate electrodes
C	equivalent circuit representation of bulk sample capacitance
C_b	blocking-layer capacitance
C_L	capacitance of microdielectrometer floating gate
$C_x(\omega)$	experimentally measured sample capacitance
C_1	constant in Williams-Landel-Ferry (WLF) equation
C_2	constant in Williams-Landel-Ferry (WLF) equation
D	dissipation factor (equivalent to $\tan\delta_x$)
$H(\omega)$	microdielectrometer transfer function
$i(t)$	time-varying current
I	complex amplitude of $i(t)$
L	spacing of parallel plate electrodes
N_i	concentration of i^{th} ion
q_i	charge of i^{th} ion
$Q(t)$	time-varying charge
r_i	radius of i^{th} ion
R	equivalent circuit representation of bulk sample resistance
$R_x(\omega)$	experimentally measured sample resistance
t_b	blocking-layer thickness
T_g	glass transition temperature
u_i	mobility of i^{th} ion
$v(t)$	time-varying voltage
V	complex amplitude of $v(t)$
$Y(\omega)$	experimentally measured admittance

REFERENCES

1. Kienle, R. H., Race, H. H.: The electrical, chemical and physical properties of alkyd resins, Trans. Electrochem. Soc., 65, 87 (1934)

2. Manegold, E., Petzoldt, W.: Die elektrische Leitfahigkeit wahrend der Reaktion von sauren bzw. alkalischen phenol-formaldehyd-Gemischen, Kolloid Z., 95, 59 (1941)

3. Lomakin, B. A., Gussewa, N. J.: Kunstoffe, 29, 145 (1939)

4. Lomakin, B. A., Gussewa, N. J.: Anwendung von Leitfahigkeits-, Viskositats- und Refraktionsmessungen zum Studium der Harzbildung, Plast. Massi, 2, 281 (1937)

5. Fineman, M. N., Puddington, I. E.: Kinetics of cure of resol resins, Ind. and Eng. Chemistry, 39, 1288 (1947)

6. Fineman, M. N., Puddington, I. E.: Measurements of cure of some thermosetting resins, Can. J. Res., Sec. B., 25, 101 (1947)

7. Coln, M. C. W., Senturia, S. D.: The application of linear system theory to parametric microsensors, p. 118, Proc. Transducers '85, 1985

8. Mopsik, F. I.: Precision time-domain dielectric spectrometer, Rev. Sci. Instr., 55, 79 (1984)

9. Aukward, J. A., Warfield, R. W.: Monitoring device for investigation of encapsulating resins, Rev. Sci. Inst., 27, 413 (1956)

10. Armstrong, R. J.: Method of laminating employing measuring the electrical impedance of a thermosetting resin, U. S. Patent No. 3,600,247.

11. Mouayad, L.: Monitoring of transformer oil using microdielectric sensors, M. S. Thesis, Massachusetts Institute of Technology, 1985, unpublished.

12. Lee, H. L.: Optimization of a resin cure sensor, M. S. Thesis, Massachusetts Institute of Technology, 1982, unpublished.

13. Senturia, S. D., Garverick, S. L.: Method and apparatus for microdielectrometry, U. S. Patent No. 4,423,371.

14. Sheppard, Jr., N. F., Garverick, S. L., Day, D. R., Senturia, S. D.: Microdielectrometry: a new method for in-situ cure monitoring, p. 65, Proc. 26th SAMPE Symposium, 1981

15. Senturia, S. D., Sheppard, Jr., N. F., Lee, H. L., Marshall, S. B.: Cure monitoring and control with combined dielectric/temperature probes, SAMPE J., 19, 22 (1983)

16. Aukward, J. A., Warfield, R. W., Petree, M. C.: Change in electrical resistivity of some high polymers during isothermal polymerization, J. Polym. Sci., 27, 199 (1958)

17. Anonymous: Dielectrics improve control of laminate cure time, Plastics Technology, 15, 19 (1969)

18. Hewlett-Packard Co., Palo Alto, CA: Manual for HP4192A Low-Frequency Impedance Analyzer.

19. GenRad Co., Concord, MA: Manual for 1689 Digibridge.

20. Micromet Instruments, Inc., Cambridge, MA: The Eumetric System II Microdielectrometer, Product Bulletin, 1985

21. McCrum, N. G., Read, B. E., Williams, G.: Anelastic and dielectric effects in polymeric solids, New York, Wiley and Sons 1967

22. Hedvig, P.: Dielectric spectroscopy of polymers, New York, Wiley and Sons 1977

23. Smyth, C. P.: Dielectric behavior and structure, New York, McGraw-Hill 1955

24. Fava, R. A., Horsfield, A. E.: The interpretation of electrical resistivity measurements during epoxy resin cure, Brit. J. Appl. Phys. (J. Phys. D), Ser. 2, 1, 117 (1968)

25. Lee, H., Neville, K.: Handbook of epoxy resins, New York, McGraw-Hill 1967

26. Wright, W. W.: Characterisation of a bisphenol-A epoxy resin, Brit. Polym. J., 15, 224 (1983)

27. Bockris, J. O'M., Reddy, A. K. N.: Modern electrochemistry, Volume 1, Section 4.4, New York, Plenum Press 1970

28. Debye, P.: Polar molecules, New York, Chemical Catalog Co. 1929

29. Cole, K. S., Cole, R. H.: Dispersion and absorption in dielectrics I. Alternating current characteristics, J. Chem. Phys., 9, 341 (1941)

30. Davidson, D. W., Cole, R. H.: Dielectric relaxation in glycerine, J. Chem. Phys., 18, 1417 (1950)

31. Williams, G., Watts, D. C.: Non-symmetrical dielectric relaxation behavior arising from a simple empirical decay function, Trans. Farad. Soc., 66, 80 (1970)

32. Williams, G., Watts, D. C., Dev, S. B., North, A. M.: Further considerations of nonsymmetrical dielectric relaxation behavior arising from a simple empirical decay function, Trans. Farad. Soc., 67, 1323 (1971)

33. Lindsey, C. P., Patterson, G. D.: Detailed comparison of the Williams-Watts and Cole-Davidson functions, J. Chem. Phys. 73, 3348 (1980)

34. Moinihan, C. T., Boesch, L. P., Laberge, N. L.: Decay function for the electric field relaxation in vitreous ionic conductors, Phys. Chem. Glasses, 14, 122 (1973)

35. Sheppard, Jr., N. F.: Dielectric analysis of the cure of thermosetting epoxy/amine systems, Ph.D. Thesis, Massachusetts Institute of Technology, 1985, unpublished.

36. Johnson, J. F., Cole, R. H.: Dielectric polarization of liquid and solid formic acid, J. Am. Chem. Soc., 73, 4536 (1951)

37. Adamec, V.: Electrical properties of an epoxy resin during and after curing, J. Polym. Sci., 10, 1277 (1972)

38. Day, D. R., Lewis, T. J., Lee, H. L., Senturia, S. D.: The role of boundary layer capacitance at blocking electrodes in the interpretation of dielectric cure data in adhesives, J. Adhesion, 18, 73 (1985)

39. Zukas, W. X., MacKnight, W. J., Schneider, N. S.: Dynamical mechanical and dielectric properties of an epoxy resin during cure, in C. A. May (ed.), Chemorheology of Thermosetting Polymers, ACS Symposium Series, 227, 223 (1983)

40. May, C. A.: Dielectric measurements for composite cure control - two case studies, p. 108, Proc. 20th SAMPE Symp., 1975

41. May, C. A.: Composite cure studies by dielectric and calorimetric analyses, p. 803, Proc. 21st SAMPE Symp., 1976

42. Lawless, G. W.: High temperature dielectric studies of epoxy resin, Polym. Eng. Sci., 20, 546 (1980)

43. Baumgartner, W. E., Ricker, T.: Computer assisted dielectric cure monitoring in material quality and cure process control, SAMPE J., 19, 6 (1983)

44. Bidstrup, W. B., Sheppard, Jr., N. F., Senturia, S. D.: Monitoring of laminate cure with microdielectrometry, SPE Tech. Papers, 31, 324 (1985)

45. Pike, R. A., Douglas, F. C., Wisner, G. R.: Electrical dissipation factor; guide to molding quality graphite/resin composites, Polym. Eng. Sci., 11, 502 (1971)

46. Sheppard, Jr., N. F., Senturia, S. D.: WLF dependence of the dielectric properties of DGEBA epoxy resins, J. Polym. Sci., Polym. Phys. Ed., submitted for publication.

47. Sheppard, Jr., N. F., Coln, M. C. W., Senturia, S. D.: A dielectric study of the time-temperature-transformation (TTT) diagram of DGEBA epoxy resins cured with DDS, p. 1243, Proc. 29th SAMPE Symp., 1984

48. Huguenin, F. G. A. E., Klein, M. T.: Intrinsic and transport-limited epoxy-amine cure kinetics, Ind. Eng. Chem. Prod. Res. Dev., 24, 166 (1985)

49. Shito, N., Sato, M.: Electrical and mechanical properties of anhydride-cured epoxy resins, J. Polym. Sci. Part C, 16, 1069 (1967)

50. Shito, N.: Specific volume, dielectric properties, and mechanical properties of cured epoxy resins in the glass-transition region, J. Polym. Sci. Part C, 23, 569 (1968)

51. Blyakhman, Ye. M., Borisova, T. I., Levitskaya, Ts.M.: Dielectric relaxation in epoxide resins hardened with different anhydrides, Polym. Sci. USSR, 12, 1756 (1970)

52. Blyakhman, Ye. M., Borisova, T. I., Levitskaya, Ts.M.: Molecular mobility study on set epoxy resins of different molecular weights, using the dielectric method, Polym. Sci. USSR, 12, 2602 (1970)

53. Williams, M. L., Landel, R. F., Ferry, J. D.: The temperature dependence of relaxation mechanisms in amorphous polymers and other glass-forming liquids, J. Am. Chem. Soc., 77, 3701 (1955)

54. Sheppard, Jr., N. F., Day, D. R., Lee, H. L., Senturia, S. D.: Microdielectrometry, Sensors & Actuators, 2, 263 (1982)

55. Delmonte, J.: Electrical properties of epoxy resins during polymerization, J. Appl. Polym. Sci., 2, 108 (1959)

56. Olyphant, Jr., M.: Effects of cure and aging on dielectric properties, Suppl. p. 12, Proc. 6th IEEE Electrical Insulation Conf., 1965

57. Warfield, R. W., Petree, M. C.: The use of electrical resistivity in the study of the polymerization of thermosetting polymers, J. Polym. Sci., 37, 305 (1959)

58. Warfield, R. W., Petree, M. C.: A study of the polymerization of epoxide polymers by electrical resistivity techniques, Polymer, 1, 178 (1960)

59. Kagan, G. T., Moshinskii, L. Ya., Nesolyonaya, L. G., Marina, D. I., Romantsevich, M. K,: Study of kinetics of setting of epoxide resins with anhydrides, Vysokomol. Soedin., A10, 62 (1968)

60. Acitelli, M. A., Prime, R. B., Sacher, E.: Kinetics of epoxy cure: (1) the system bisphenol-A diglycidyl ether/m-phenylene diamine, Polymer, 12, 335 (1971)

61. Prime, R. B.: Thermosets, in Edith Turi (ed.), Thermal Characterization of Polymeric Materials, New York, Academic Press 1981

62. Schechter, L., Wynstra, J., Kurkjy, R. P.: Glycidyl ether reactions with amines, Ind. Eng. Chem., 48, 94 (1956)

63. Sourour, S., Kamal, M. R.: Differential scanning calorimetry of epoxy cure: isothermal cure kinetics, Thermochimica Acta, 14, 41 (1976)

64. Judd, N. C. W.: Investigation of the polymerization of an unsaturated polyester system by a resistivity technique, J. Appl. Polym. Sci., 9, 1743 (1965)

65. Learmonth, G. S., Pritchard, G.: Electrical resistivity and crosslinking in thermosetting resins, Ind. Eng. Chem. Prod. Res. Dev., 8, 124 (1969)

66. Fisch, W., Hofmann, W.: Chemischer Aufbau von gaherteten Epoxyharzen, Makromol. Chem, 44, 8 (1961)

67. Huraux, C., Sellaimia, A.: Variation des proprietes dielectriques accompagnant le durcissement de resines epoxydes, C. R. Acad. Sc. Paris, 277, Serie B, 497 (1973)

68. Huraux, C., Sellaimia, A.: Sur la variation des proprieties dielectriques et la cinetique du durcissement de resines epoxides, C. R. Acad. Sc. Paris, 277, Serie B, 691 (1973)

69. Dandurant, D., Huraux, C.: Etude de mecanisme de durcissement de resines au moyen de spectres de relaxation dielectrique, Prace Naukowe Instytutu Podstaw Elektrotechniki i Electrotechnologii Politechniki Wrocleawskiej, 16, 275 (1977)

70. Soualmia, A., Huraux, C., Despax, B.: Relation entre les parametres dieleletriques et la cinetique de reaction de polymerisation en phase liquide, Makromol. Chem., 183, 1803 (1982)

71. Sheppard, Jr., N. F., Senturia, S. D.: Chemical interpretation of the relaxed permittivity during epoxy resin cure, SPE Tech. Papers, 31, 321 (1985)

72. Williams, G.: Dielectric information on chain mobility, chain configuration, and an order-disorder transition in amorphous poly(acetaldehyde), Trans. Farad. Soc., 59, 1397 (1962)

73. Sheppard, Jr., N. F., Senturia, S. D.: Molecular contributions to the dielectric permittivity of unreacted epoxy/amine mixtures, p. 22a, Technical Program Summary, Adhesion Society Annual Meeting, Savannah, GA, 1985

74. Lane, J. W., Bachmann, M. S., Seferis, J. C.: Monitoring of matrix property changes during composite processing, SPE Tech. Papers, 31, 318 (1985)

75. Lane, J. W., Bachmann, M. S., Seferis, J. C.: Dielectric Studies of the cure of epoxy matrix systems, J. Appl. Polym. Sci., in press.

76. Tajima, Y. A., Crozier, D.: Thermokinetic modeling of an epoxy resin I. Chemoviscosity, Polym. Eng. Sci., 23, 186 (1983)

77. Apicella, A., Nicolais, L., Nobile, M. R., Castiglione-Morelli, M. A.: Effect of processing variables on the durability of epoxy resins for composite systems, Comp. Sci. Tech., in press.

78. Enns, J. B., Gillham, J. K.: Time-temperature-transformation (TTT) cure diagram: modeling the cure behavior of thermosets, J. Appl. Polym. Sci., 28, 2567 (1983)

79. Zukas, W. X., Schneider, N. S., MacKnight, W. J.: Dielectric and dynamic mechanical monitoring of epoxy resin cure, Polym. Prepr., 25(2), 205 (1984)

80. Daly, J., Pethrick, R. A.: Rubber-modified epoxy resins: 2. Dielectric and ultrasonic relaxation studies, Polymer, 22, 37 (1981)

81. Sacher, E.: The DC conductivity of polyimide film, p. 33, Proc. IEEE Conf. on Elec. Ins. Dielec. Phen., 1976

82. Carpenter, J. F.: Instrumental techniques for developing epoxy cure cycles, p. 783, Proc. 21st SAMPE Symposium, 1976

83. Tajima, Y. A.: Monitoring cure viscosity of epoxy composite, Polym. Comp., 3, 162 (1982)

84. Kranbuehl, D. E.: Dynamic dielectric characterization of thermosets and thermoplastics using intrinsic variables, p. 1251, Proc. 29th SAMPE Symp., 1984

85. Kranbuehl, D. E., Delos, S., Yi, E., Mayer, J., Hou, T., Winfree, W.: Correlation of dynamic dielectric measurements with viscosity in polymeric resin systems, p. 638, Proc. 30th SAMPE Symp., 1985

86. McGowan, E. J., Mathes, K. N.: Measurement of cure in casting resins by means of electrical properties, p. 17, Proc. IEEE Conf. on Elec. Insul., 1962

87. Adabbo, H. E., Williams, R. J. J.: The evolution of thermosetting polymers in a conversion-temperature phase diagram, J. Appl. Polym. Sci. 27, 1327 (1982)

88. Armstrong, R. J.: Laminating control system, Solid State Technology, p. 50, Nov. 1969

89. Kim, D. H.: Application of the dielectric analysis to polymeric materials control, Proc. TTCP-3 Critical Review; Techniques for the Characterization of Polymeric Materials, AMMRC MS 77-2, AD-36082, 1977

90. Dixon, R. R.: Measuring moisture by dielectric analysis, SPE Tech. Papers, 25, 835 (1979)

91. May, C. A., Hadad, D. K., Browning, C. E.: Physiochemical quality assurance methods for composite matrix resins, Polym. Eng. Sci., 19, 545 (1979)

92. Standish, J. V., Leidheiser, Jr., H.: The effect of water on the dielectric properties of a corrosion-protective epoxy-polyamide coating, ACS Div. Org. Coat. Plast. Chem. Prepr. 43, 565 (1980)

93. Day, D. R.: Effects of stoichiometric mixing ratio on epoxy cure - a dielectric analysis, SPE Tech. Papers, 31, 327 (1985)

94. Senturia, S. D., Sheppard, Jr., N. F., Lee, H. L., Day, D. R.: In-situ measurement of the properties of curing systems with microdielectrometry, J. Adhesion, 15, 69 (1982)

95. May, C. A., Dusi, M. R., Fritzen, J. S., Hadad, D. K., Maximovich, M. G., Thrasher, K. G., Wereta, Jr., A.: A rheological and chemical overview of thermoset curing, in C. A. May (ed.), Chemorheology of Thermosetting Polymers, ACS Symposium Series 227, 1 (1983)

96. Chottiner, J., Sanjana, Z. N., Kodani, M. R., Lengel, K. W., Rosenblatt, G. B.: Monitoring cure of large autoclave molded parts by dielectric analysis, p. 77, Proc. 26th SAMPE Symp., 1981

97. Sanjana, Z. N., Selby, R. L.: Monitoring cure of epoxy resins using a microdielectrometer, p. 1233, Proc. 29th SAMPE Symp., 1984

98. Allen, J. D.: In-process dielectric monitoring of polymeric resin cure, p. 270, Proc. 20th SAMPE Symp., 1975

99. Crabtree, D. J.: Ion graphing as an in-process cure monitoring procedure for composite and adhesively bonded structures, p. 636, Proc. 22nd SAMPE Symp., 1977

100. Sanjana, Z. N., Schaefer, W. H., Ray, J. R.: Effect of aging and moisture on the reactivity of a graphite epoxy prepreg, Polym. Eng. Sci., 21, 474 (1981)

101. Weresta, Jr., A., May, C. A.: Dielectric monitoring of the bonding process, J. Adhesion, 12, 317 (1981)

102. Pike, R. A., Lamm, F. P., Pinto, J. P.: Factors affecting the processing of epoxy film adhesives: 1. Room temperature aging, J. Adhesion, 12, 143 (1981)

103. La Mantia, F. P., Schifani, R., Acierno, D.: Effect of a filler on the dielectric properties of an epoxy resin, J. Appl. Polym. Sci., 28, 3075 (1983)

104. Delmonte, J.: Elctrical properties of modified epoxy resins, Modern Plastics, 35, 152 (1958)

105. Sanjana, Z. N., Selby, R. L.: The use of dielectric analysis to study the cure of a filled epoxy resin, IEEE Trans. Elec. Ins., 16, 496 (1981)

106. Pais, J. C., Griffiths, V. S.: The effect of chemical bonding on current flow in thermosetting polymers, p. 5, Proc. IEEE Conf. on Elec. Insul. and Dielec. Phen., 1968

107. Learmonth, G. S., Tomlinson, F. M., Czerski, J.: Cure of polyester resins, I., J. Appl. Polym. Sci., 12, 403 (1968)

108. Learmonth, G. S., Pritchard, G.: Dielectric relaxation and crosslinking in unsaturated polyester resins, J. Appl. Polym. Sci., 13, 1219 (1969)

109. Van Beek, L. K. H.: Dielectric behavior of curing phenolic-formaldehyde resins, J. Appl. Polym. Sci., 8, 2843 (1964)

110. Sanjana, Z. N.: A study of wire enamel cure using dielectric analysis, Proc. IEEE Conf. Electr. and Electronic Insul., 15, 150 (1981)

111. Kranbuehl, D. E., Delos, S., Jue, P. K.: Dynamic dielectric characterization of the cure process: LARC-160, SAMPE J., 19, 18 (1983)

112. Kranbuehl, D. E., Delos, S., Yi, E.: Dynamic dielectric analysis: nondestructive material evaluation and cure cycle monitoring, SPE Tech. Papers, 31, 311 (1985)

113. Krishna, J. G., Josylu, O. S., Sobhanadri, J., Subrahmaniam, R.: Dielectric behavior of isocyanate-terminated polymers, J. Phys. D: Appl. Phys., 15, 2315 (1982)

114. Goswami, D. N.: The dielectric behavior of natural resin shellac, J. Appl. Polym. Sci., 23, 529 (1979)

115. Khastgir, D., Ghoshal, P. K., Das, C. K.: Dielectric behavior and sulphur vulcanization of the crosslinked butyl (XL-50) rubber, Polymer, 24, 617 (1983)

116. Hinkley, J. A.: Monitoring of a rubber cure by microdielectrometry, U. S. Naval Research Lab Memorandum Report 5300, March 30, 1984

117. Wereta, Jr., A., May, C. A.: Dielectric cure investigation of acetylene terminated oligomers, ACS Div. Org. Coat. Plast. Chem. Prepr., 38, 679 (1978)

118. Sanjana, Z. N.: Overage indicators for prepreg products, SAMPE J., 16, 5 (1980)

TABLE I BIBLIOGRAPHIC REFERENCES BY MATERIALS STUDIED

RESINS

EPOXIES

Pure Epoxies
46,69

DGEBA, Amine cured
41,47,54,55,58,60,67,68,70,71,73,93,94

DGEBA, Anhydride cured
49,50,51,52,55,56,58,96,104

DGEBA, Other curing agents
41,44,74,75,84,85,92,105,112

Tetrafunctional Aerospace resins
39,40,41,42,43,44,45,74,75,79,82,83,84,91,95,97,98,99,100, 101,118

Other epoxies including rubber-modified and novolac resins
37,40,80,86,88,89,90,91,96,97,101,102,103,105

POLYESTERS
57,64,65,106,107,108,110

PHENOLICS
2,5,6,109

POLYIMIDES
41,45,84,95,101,111,112

POLYURETHANES
69,113

RUBBER
115,116

SHELLAC AND OTHER RESINS
114,117

COMPOSITES

EPOXY-GLASS
40,43,44,88,89,90,91,96,98

EPOXY-GRAPHITE
40,42,44,45,82,83,91,95,98,99,100,118

EPOXY WITH OTHER FIBERS AND FILLERS
102,103,105

POLYIMIDE-GRAPHITE
112

TABLE II BIBLIOGRAPHIC REFERENCES BY APPLICATION AND DATA TYPE

APPLICATION

CURE RATE AND/OR CATALYST STUDIES
37,39,40,41,56,57,58,60,64,65,67,68,69,70,71,79,91,93,94,95,
97,100,105,108,111,112

CORRELATIONS WITH MECHANICAL PROPERTIES
39,42,43,47,54,55,60,67,68,70,74,75,79,82,83,85,88,95,100,
107,115

MOISTURE EFFECTS
90,92,100,109,118

AGING EFFECTS
40,83,91,95,100,102,111,112,118

GENERAL PROCESS MONITORING
40,41,42,43,44,45,82,83,84,86,88,89,90,91,95,96,97,98,99,100,
101(bond lines),110(wire coating),113,116,117

POST-CURE STUDIES
49,50,51,52,56,57,58,80,84,86,92,93,94,100,103,104,109,111,
113,114

DATA TYPE

CONDUCTIVITY AND/OR LOSS FACTOR
2,5,6,37,39,44,46,47,49,50,54,57,58,60,64,65,67,68,69,70,
74,75,79,80,82,83,84,85,86,88,89,92,93,94,97,99,103,106,107,109,
112,113,114,115,116

PERMITTIVITY
37,39,46,47,49,50,51,52,54,55,56,67,68,69,70,71,73,74,75,79,80,
84,85,92,93,94,97,103,104,108,109,112,113,114

DISSIPATION FACTOR
40,41,42,43,45,51,52,55,56,82,83,84,89,90,91,92,95,96,98,100,
102,104,105,108,110,111,112,115,117,118

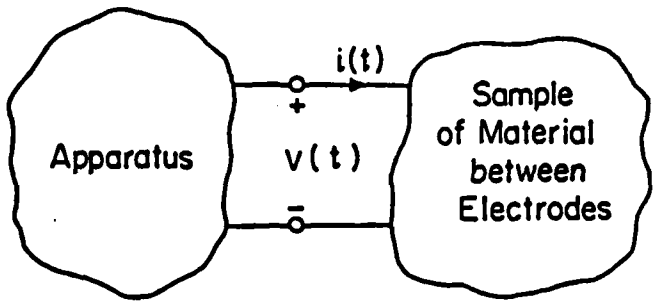

Figure 1 "Black-box" view of dielectric measurement. Apparatus applies a time-varying voltage v(t) to the electrodes and measures the time-varying current i(t).

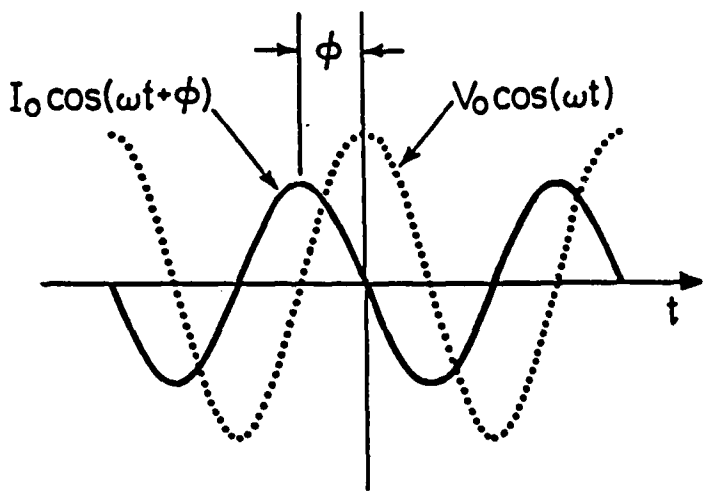

Figure 2 Sinusoidal voltage and current waveforms having a phase difference ϕ.

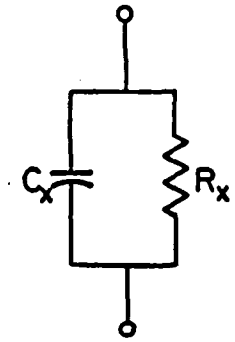

Figure 3 Equivalent circuit for the admittance of the electrodes and sample of Figure 1.

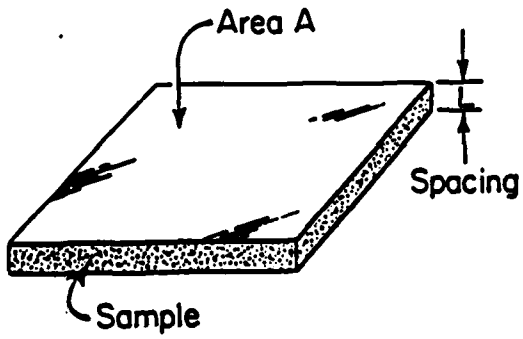

Figure 4 Parallel plate electrodes.

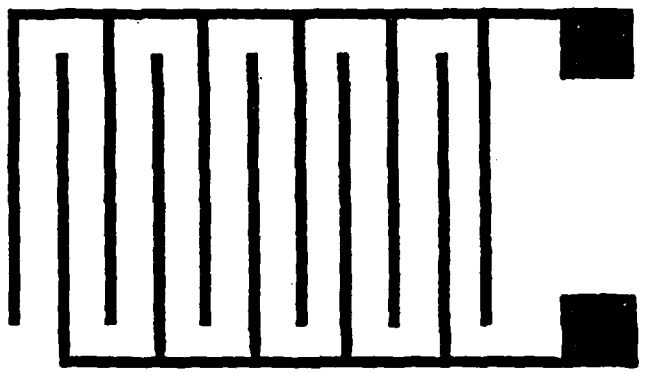

(a)

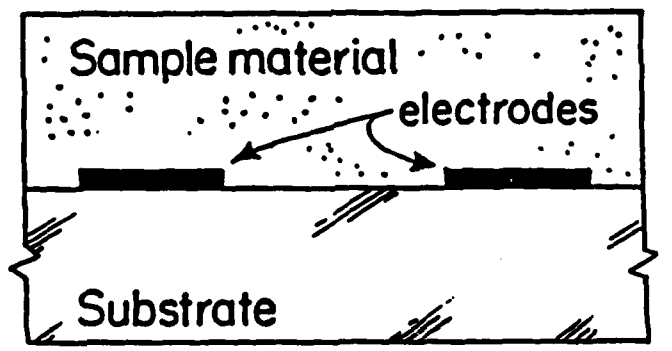

(b)

Figure 5 a) Top view of comb electrodes. b) Cross-section where the insulating substrate is much thicker than the electrode spacing.

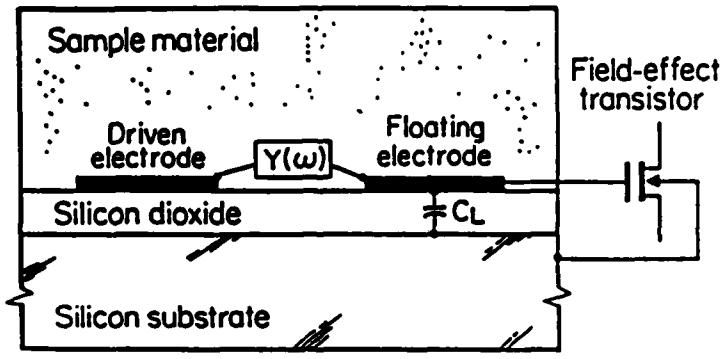

Figure 6 Cross-section of microdielectrometer sensor. The silicon dioxide insulator is much thinner than the electrode spacing. $Y(\omega)$ is the comb electrode admittance; C_L is the capacitance between the floating electrode and the substrate.

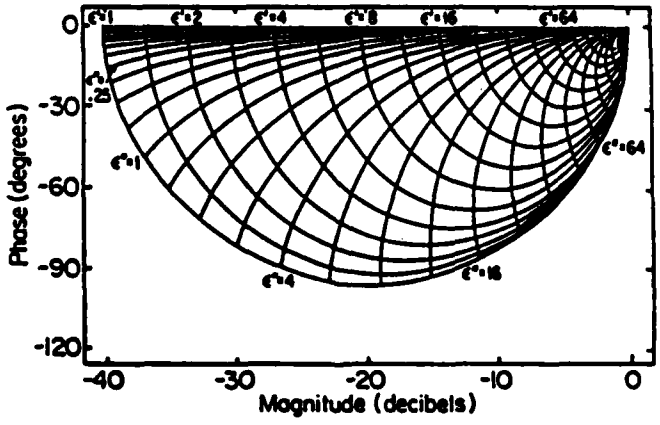

Figure 7 Calibration of the microdielectrometer sensor, showing contours of constant permittivity and loss factor as a function of the magnitude and phase of the transfer function $H(\omega)$. (Reprinted from [7] with permission of IEEE, © 1985 IEEE.)

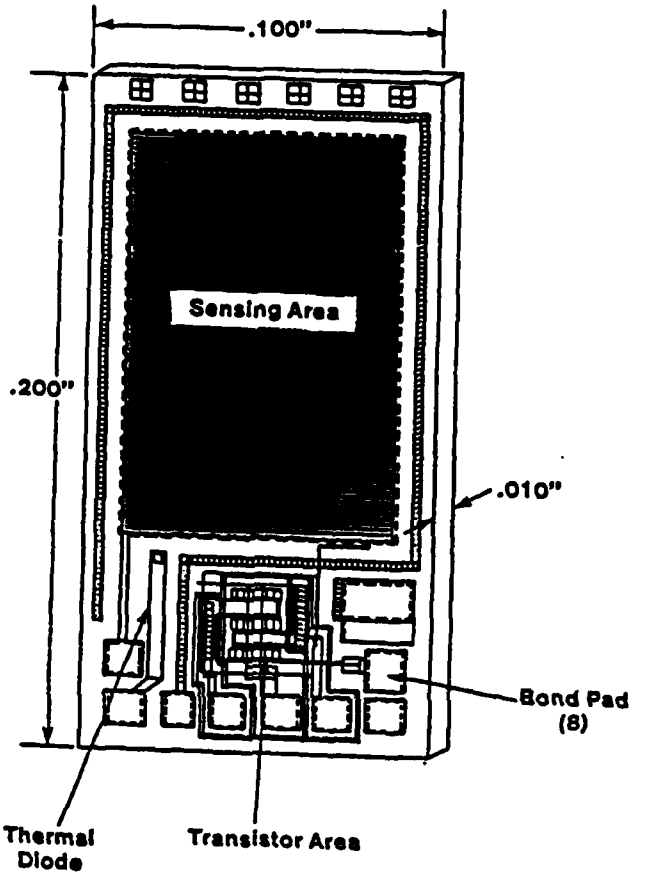

Figure 8 Schematic top view of actual microdielectrometer sensor, illustrating the comb electrode structure, field effect transistors and thermal diode temperature indicator. (Reprinted with permission of Micromet Instruments, Inc.)

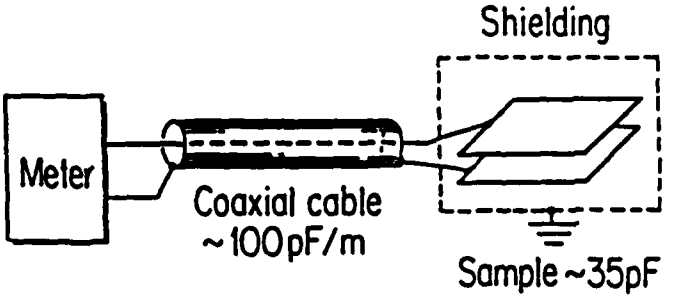

Figure 9 Schematic diagram of admittance measurement.

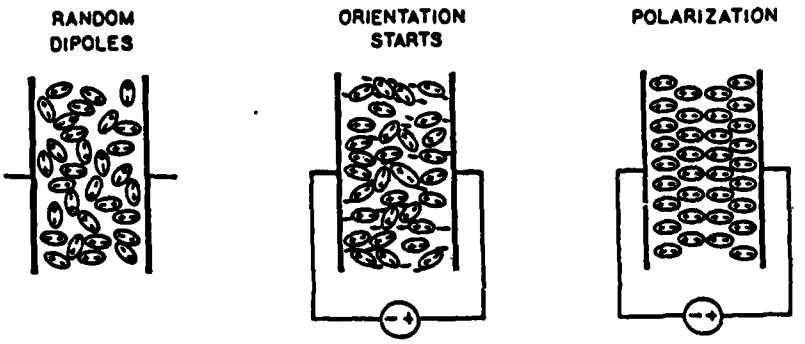

Figure 10 Schematic illustration of dipole orientation process in the presence of an applied electric field. (Reprinted from [38] with permission of Gordon and Breach Science Publishers.)

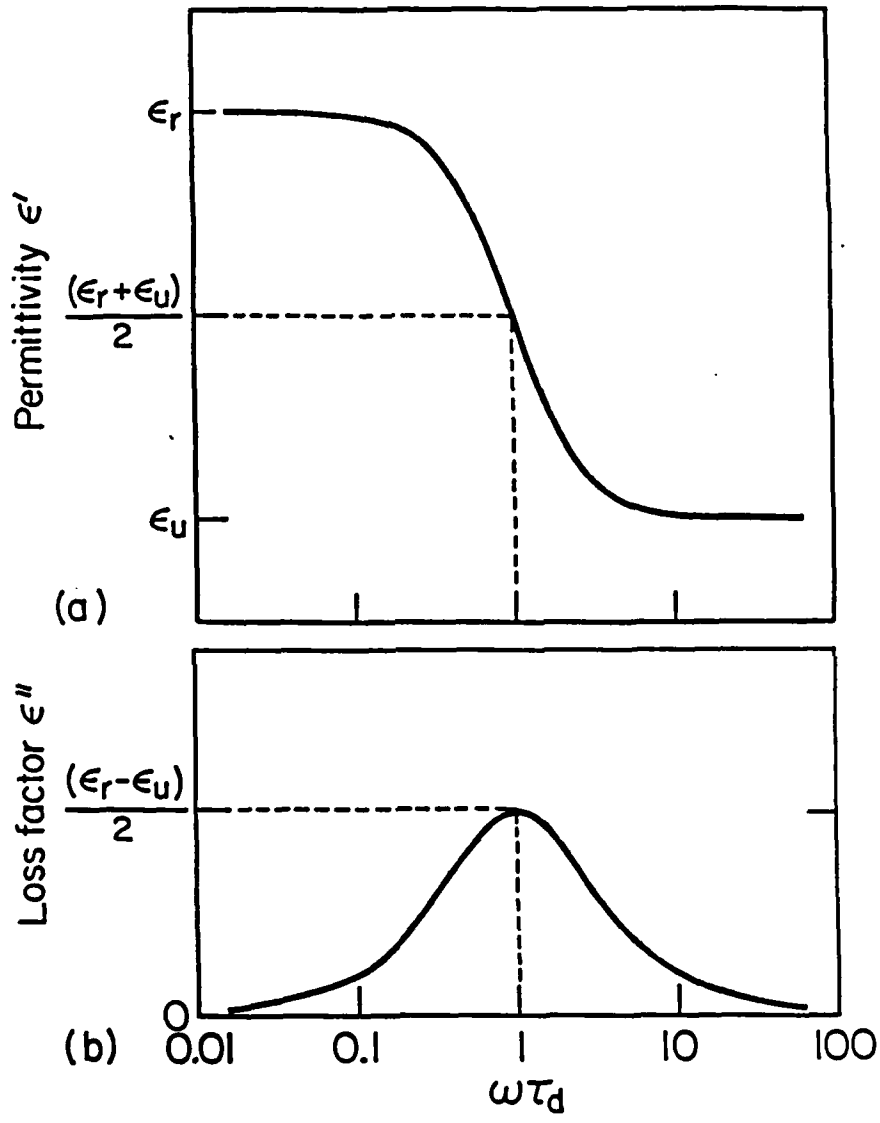

Figure 11 Debye single relaxation time model for dipole orientation showing (a) permittivity and (b) loss factor as a function of the product of the angular frequency ω and the dipole relaxation time τ_d. The relaxed permittivity is ε_r and the unrelaxed permittivity is ε_u.

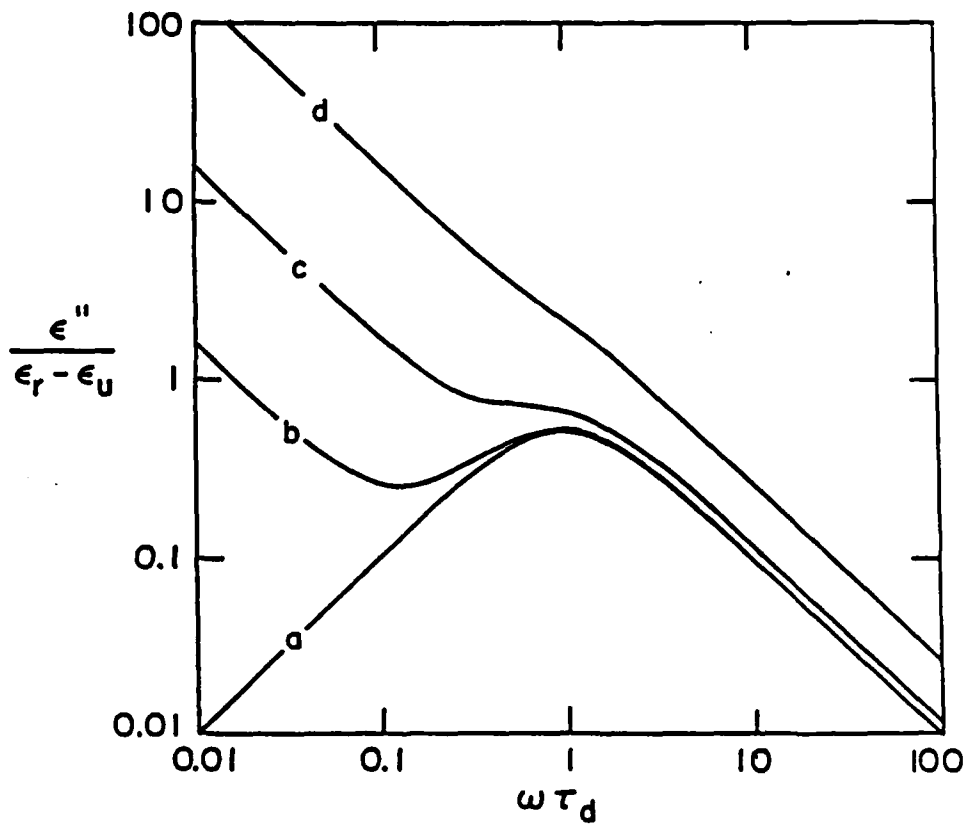

Figure 12 Illustration of the effect of conductivity σ on the frequency dependence of the loss factor.
a) $\sigma = 0$; b),c),d) $\sigma / [(\epsilon_r - \epsilon_u)\epsilon_0] = 0.1, 1, 10$.

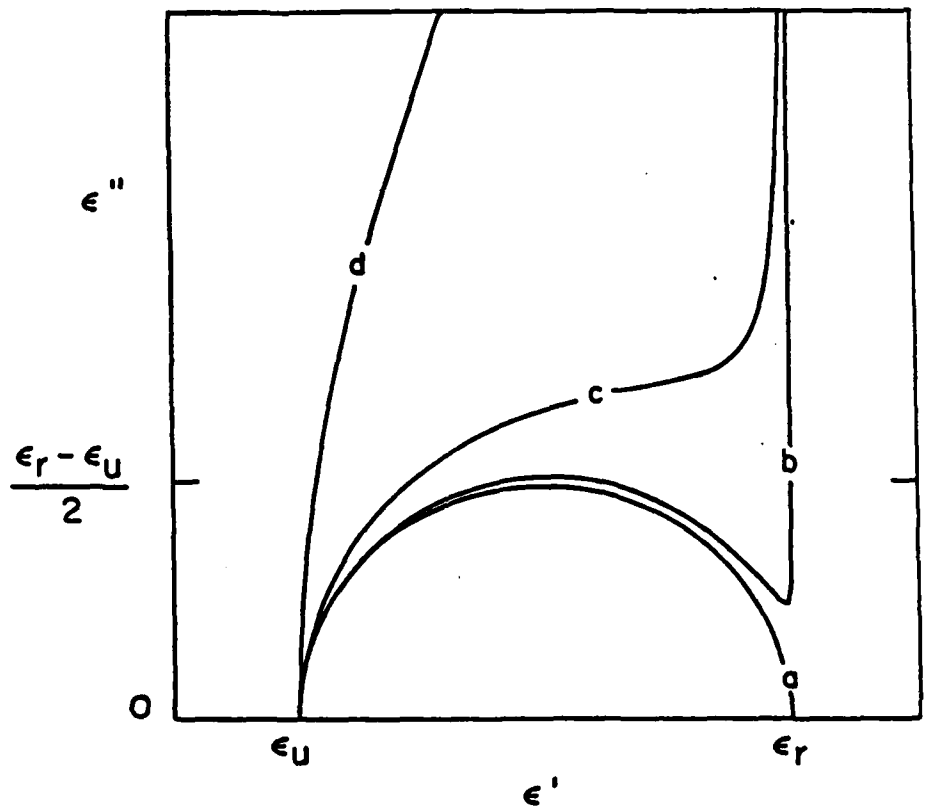

Figure 13 Cole-Cole diagram illustrating effect of varying conductivity levels as in Figure 12. Permittivity is from Figure 11a.

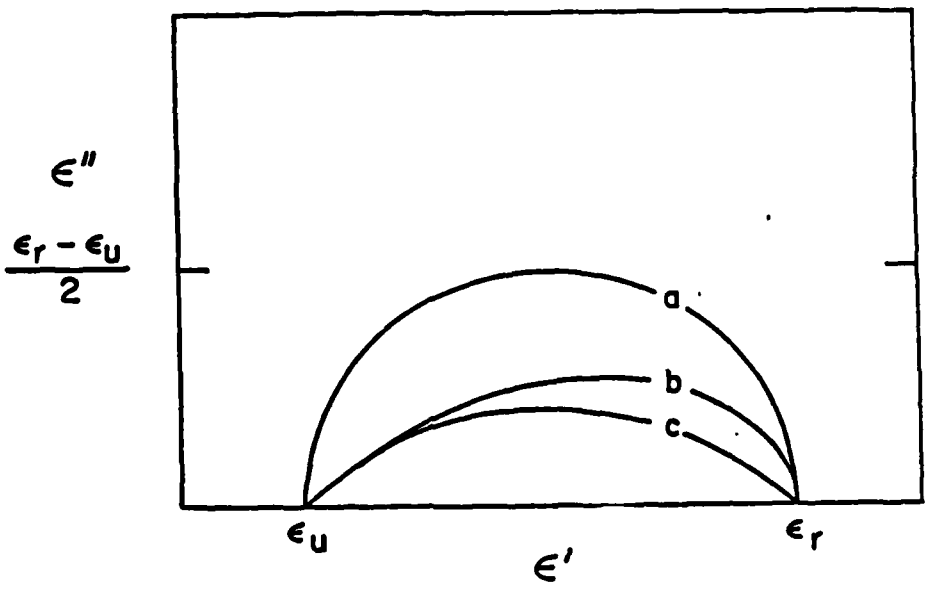

Figure 14 Cole-Cole diagrams illustrating dipole relaxation behavior. a) Debye single relaxation time model. b) Williams-Watts expression with β=0.5. c) Cole-Cole expression with β=0.5.

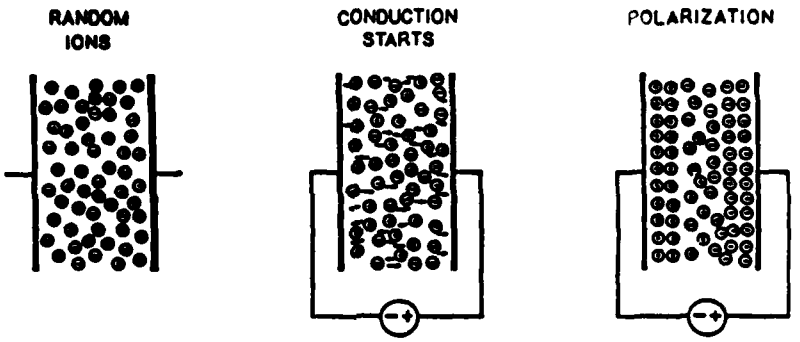

Figure 15 Schematic illustration of ion conduction in the presence of an applied electric field leading to electrode polarization. (Reprinted from [38] with permission of Gordon and Breach Science Publishers.)

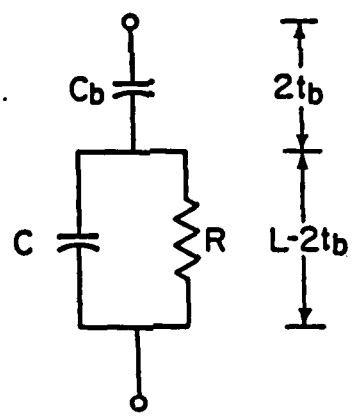

Figure 16 Equivalent circuit for the electrode admittance in the presence of electrode polarization. (Reprinted from [38] with permission of Gordon and Breach Science Publishers.)

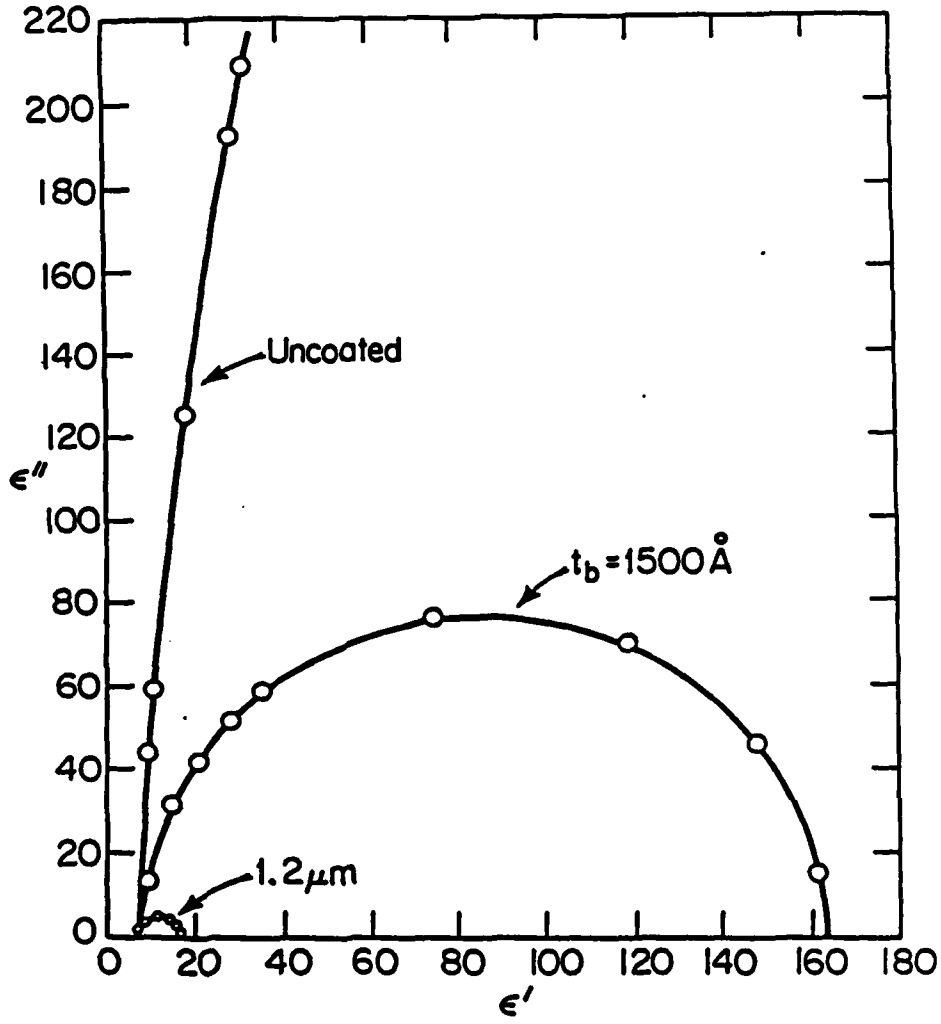

Figure 17 Cole-Cole diagram of the dielectric properties of a DGEBA epoxy resin measured on a microdielectrometer sensor with blocking layers of indicated thickness. (Reprinted from [38] with permission of Gordon and Breach Science Publishers.)

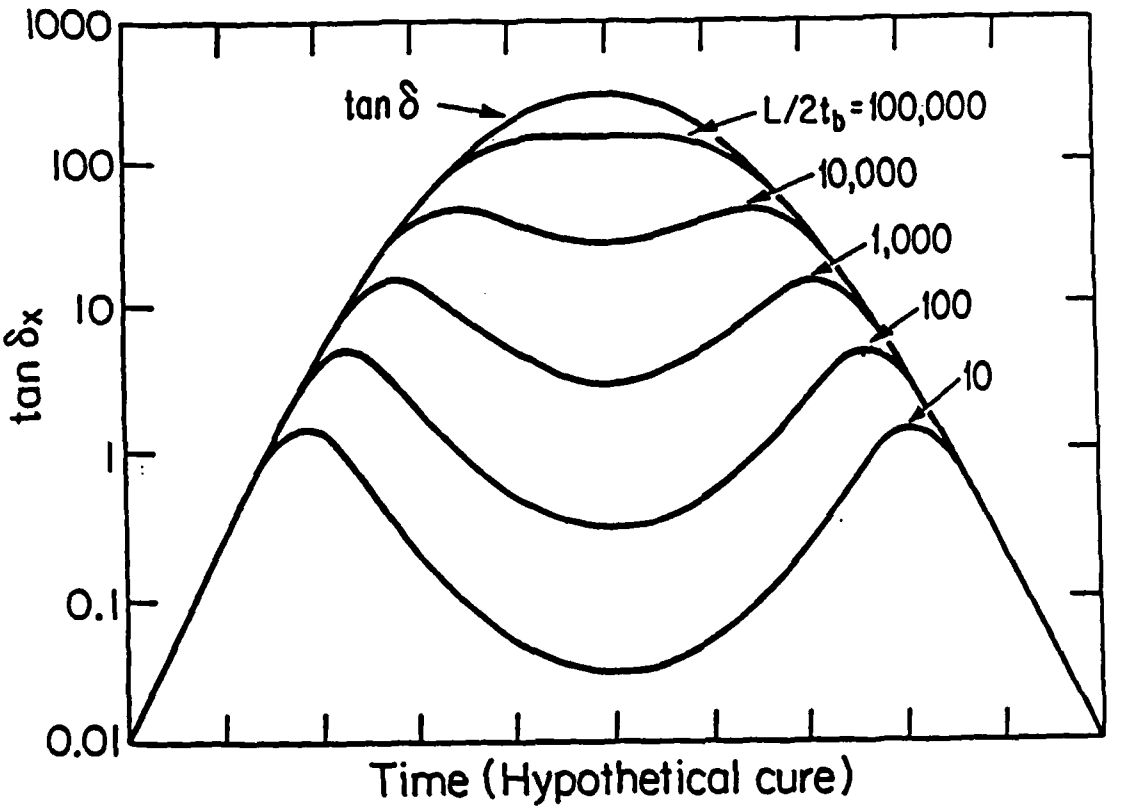

Figure 18 Schematic illustration of loss tangent behavior during a hypothetical cure for indicated values of the ratio $L/2t_b$. (Reprinted from [38] with permission of Gordon and Breach Science Publishers.)

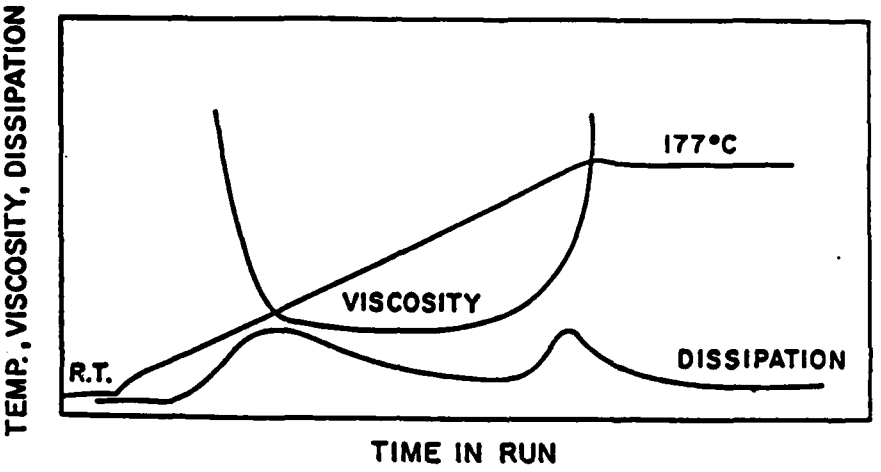

Figure 19 Plot of viscosity and dissipation factor during cure of an epoxy resin illustrating "camel-back" in dissipation factor and the correspondance of the minimum viscosity with the minimum between the two dissipation factor peaks. (Reprinted from [42] with permission of the Society of Plastics Engineers.)

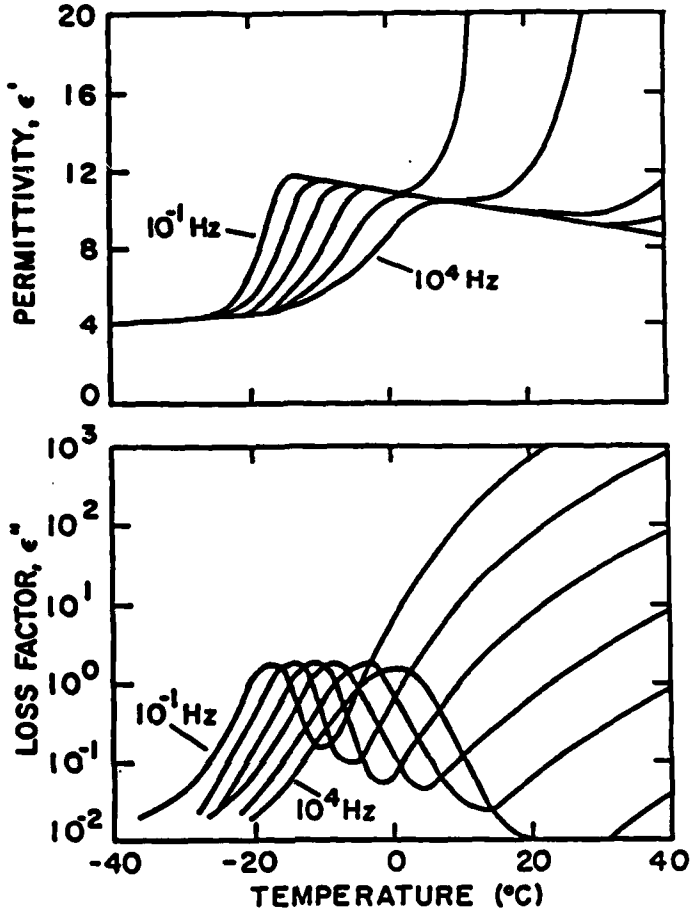

Figure 20 Plot of permittivity and loss factor versus temperature for EPON 828 resin in the vicinity of the glass transition. (Reprinted from [46] with permission of the authors.)

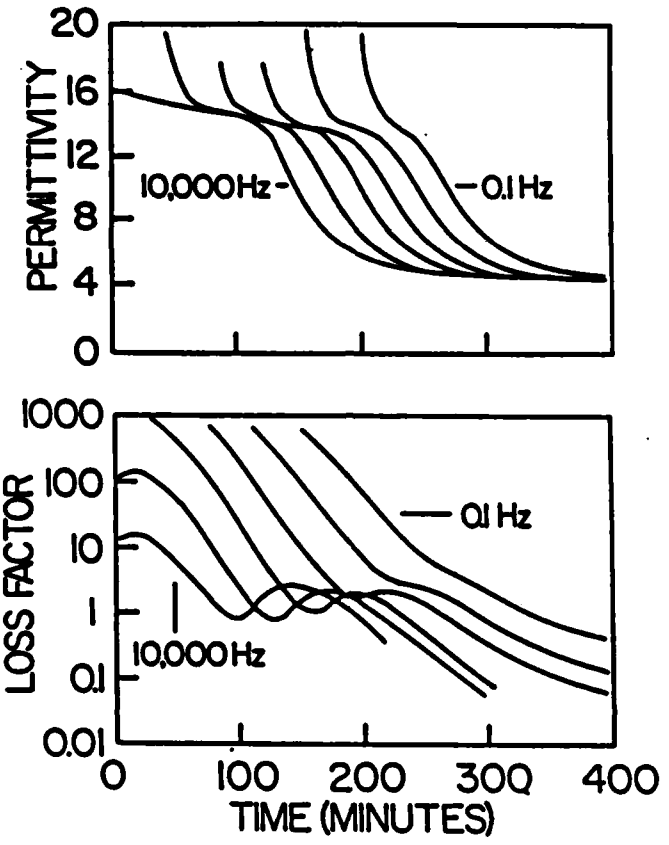

Figure 21 Plot of permittivity and loss factor versus time during the cure of a low molecular weight DGEBA resin (EPON 825) with DDS at 137 °C. (Reprinted from [47] with permission of the Society for the Advancement of Material and Process Engineering.)

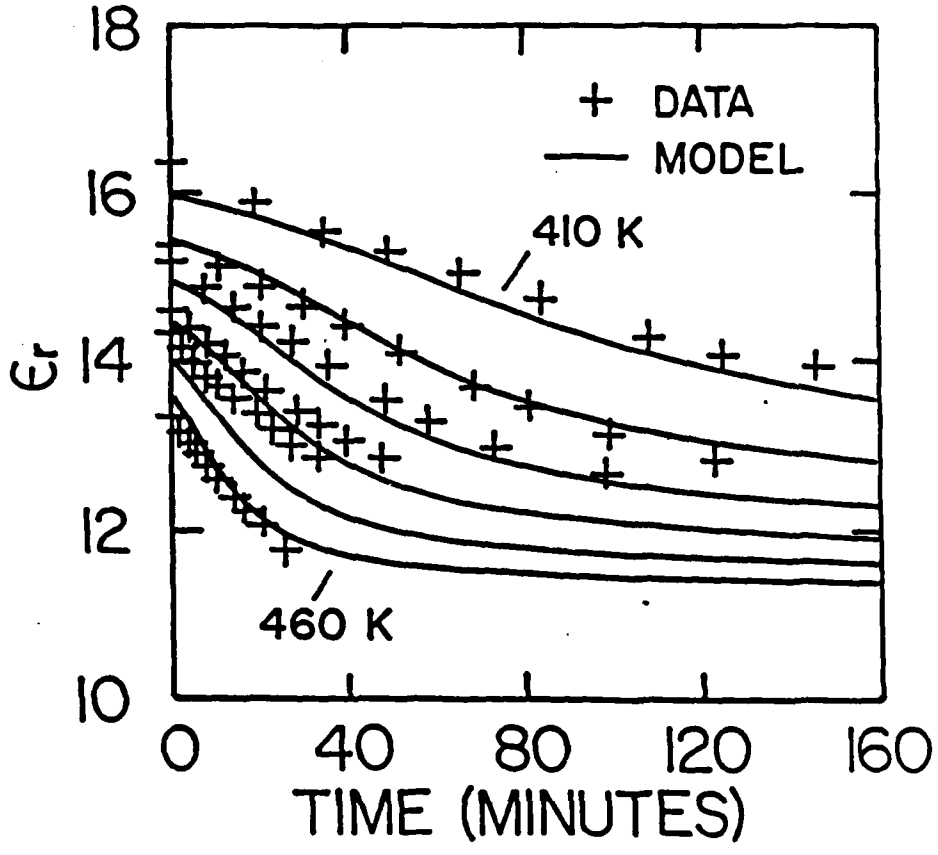

Figure 22 Plot of relaxed permittivity versus time for a low molecular weight DGEBA resin (EPON 825) cured isothermally with DDS at temperatures between 410K and 460K. Crosses represent experimental data; the solid curve represents the model described in the text. (Reprinted from [71] with permission of the Society of Plastics Engineers.)

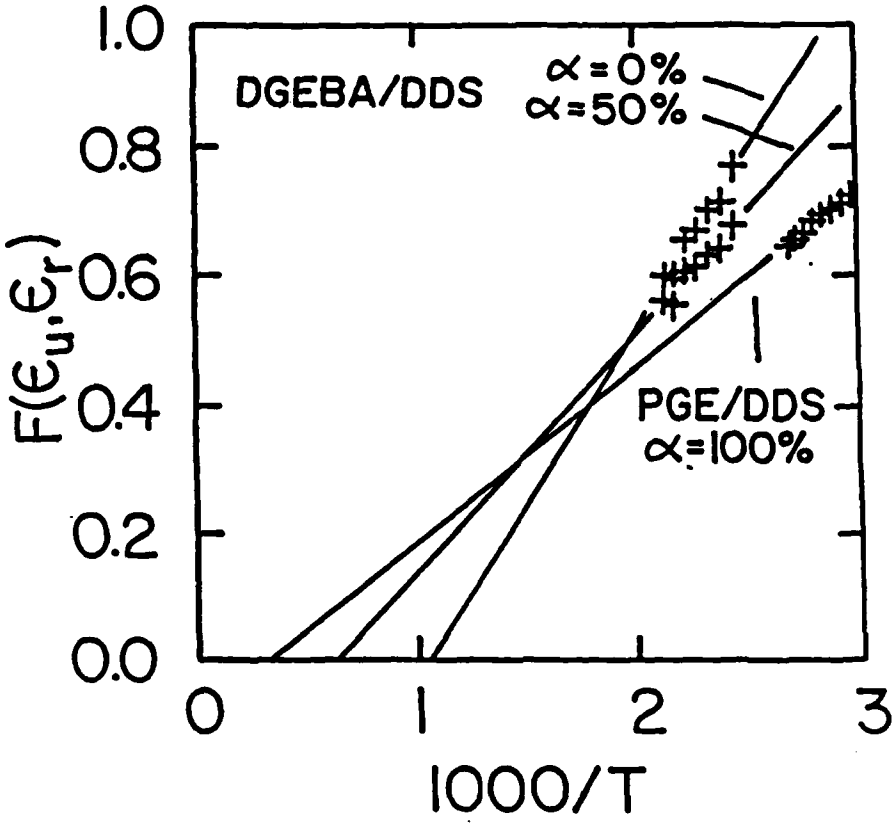

Figure 23 Test plot of the Onsager relation (Eq. D-2) for the data of Figure 22 at different extents of conversion as determined by DSC measurements. (Reprinted from [71] with permission of the Society of Plastics Engineers.)

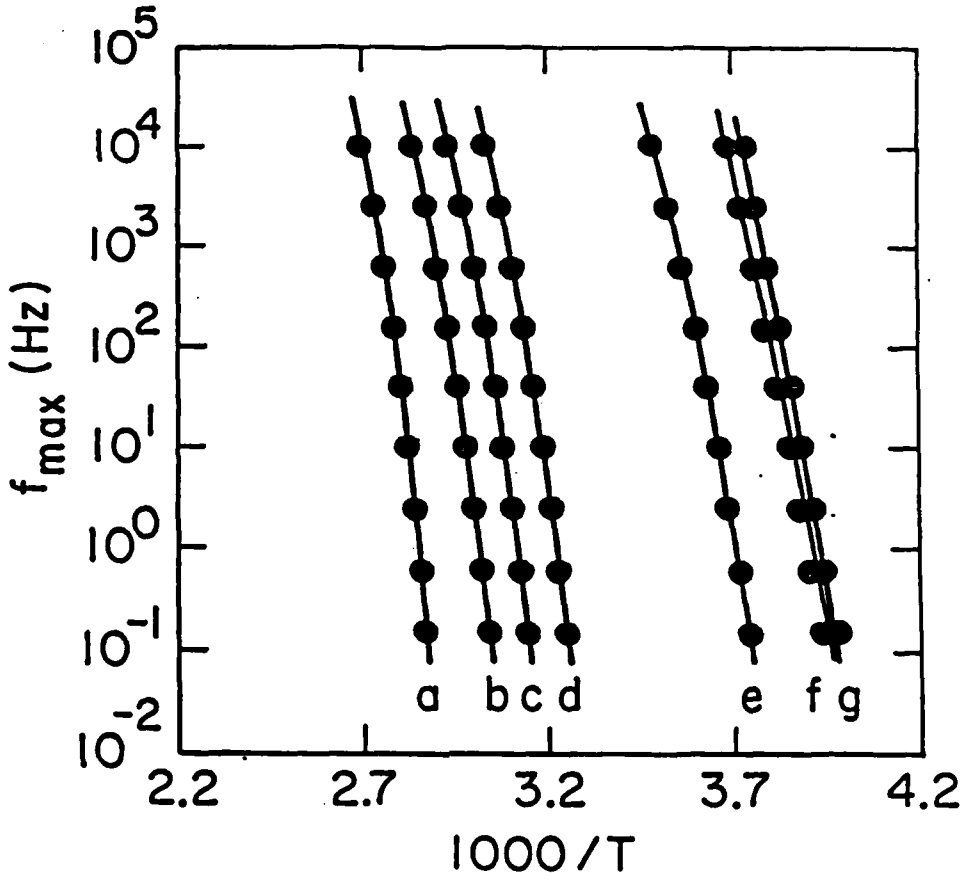

Figure 24 Arrhenius plot of the frequency of maximum dipole loss for DGEBA epoxy resins of varying molecular weights. a) n=12.1; b) 5.1; c) 3.4; d) 2.1; e) 0.6; f) 0.2; g) 0. (Reprinted from [46] with permission of the authors.)

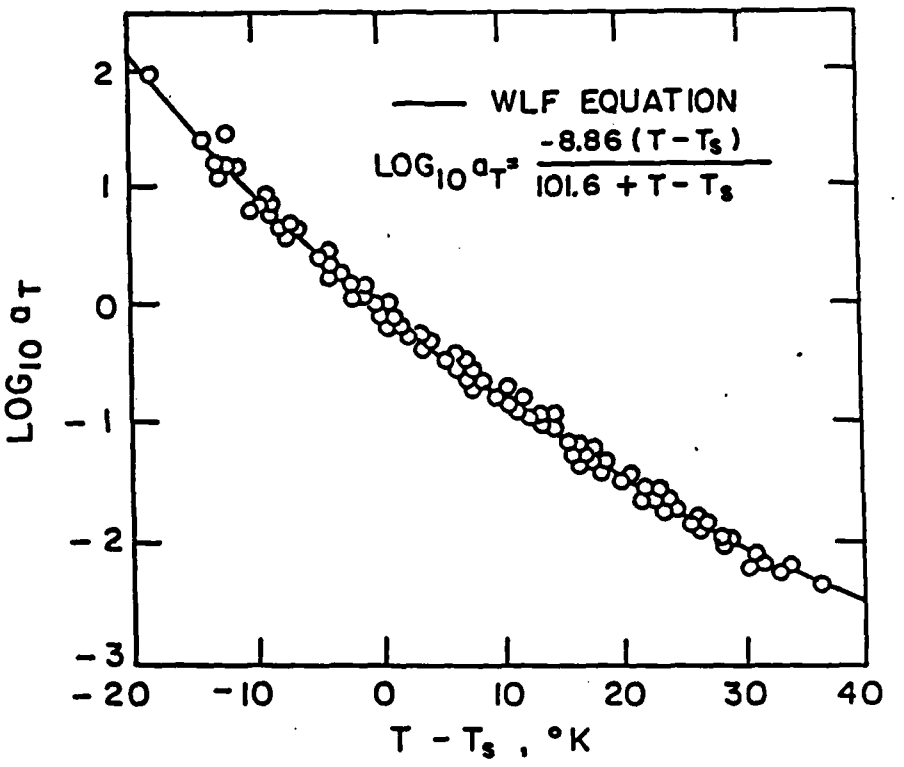

Figure 25 Shito's test plot of the Williams-Landel-Ferry equation for the dipole relaxation time in an anhydride-cured epoxy. (Reprinted from [50] with permission of John Wiley and Sons, Inc.)

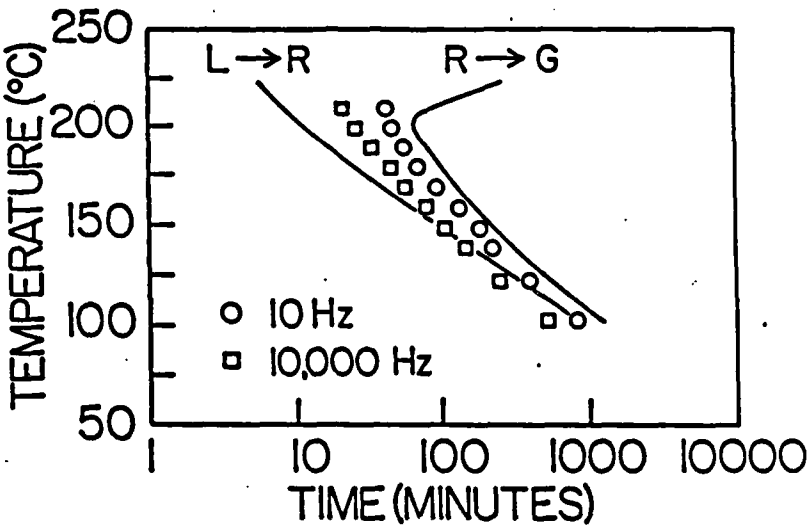

Figure 26 Time-temperature-transformation diagram for the system EPON 825/DDS showing times to reach dipole loss peaks at 10 and 10,000 Hz. (Reprinted from [47] with permission of the Society for the Advancement of Material and Process Engineering.)

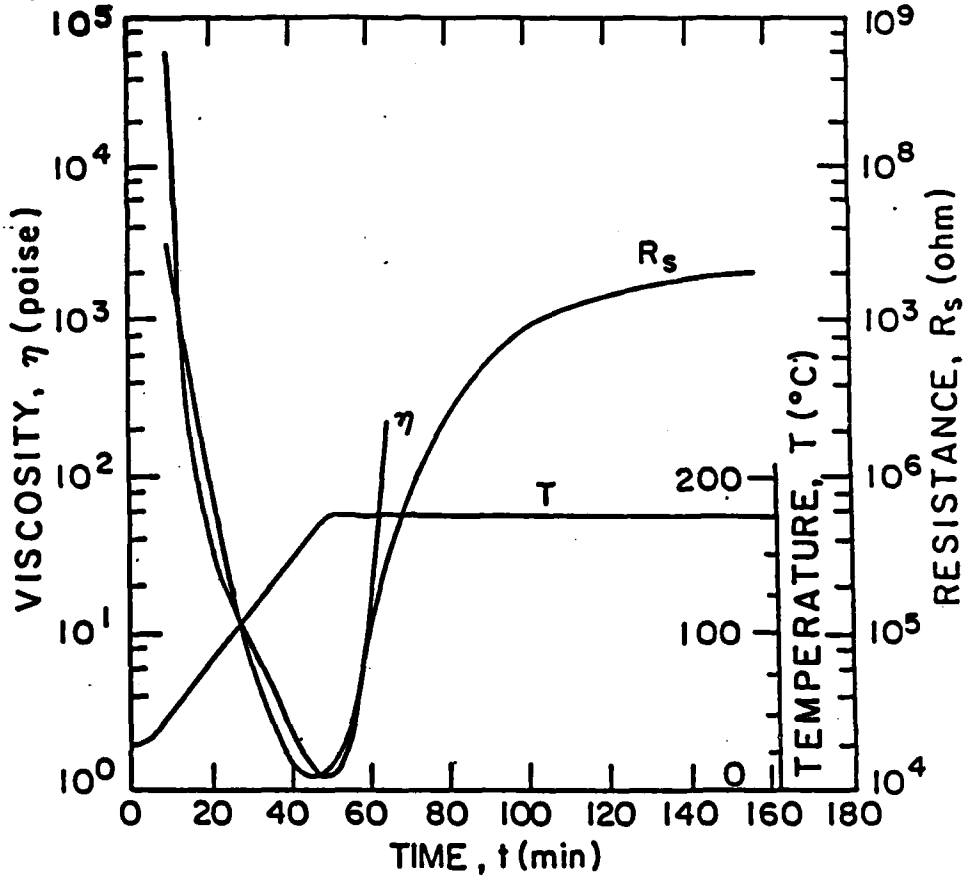

Figure 27 Tajima's plot of viscosity and resistance during the cure of an epoxy resin. (Reprinted from [76] with permission of the Society of Plastics Engineers.)

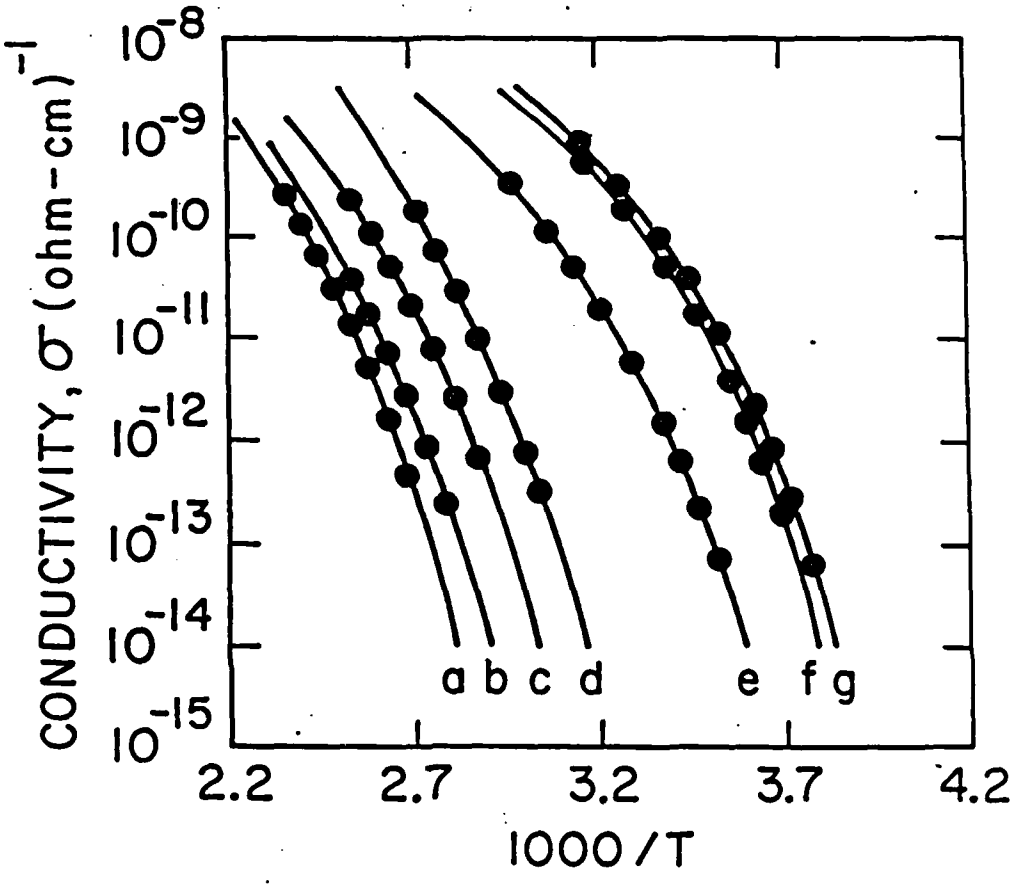

Figure 28 Arrhenius plot of the conductivity for DGEBA epoxy resins of varying molecular weights. a) n=12.1; b) 5.1; c) 3.4; d) 2.1; e) 0.6; f) n=0.2; g) 0. (Reprinted from [46] with permission of the authors.)

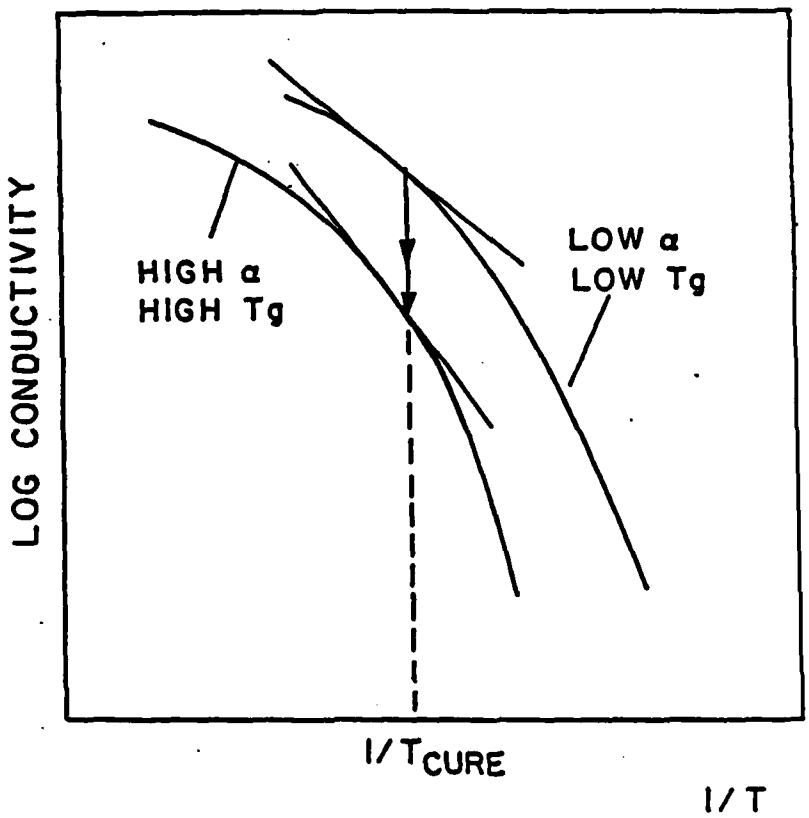

Figure 29 Schematic illustration of the temperature dependence of the conductivity during two points of an isothermal thermoset cure. (Reprinted from [35] with permission of the Massachusetts Institute of Technology.)

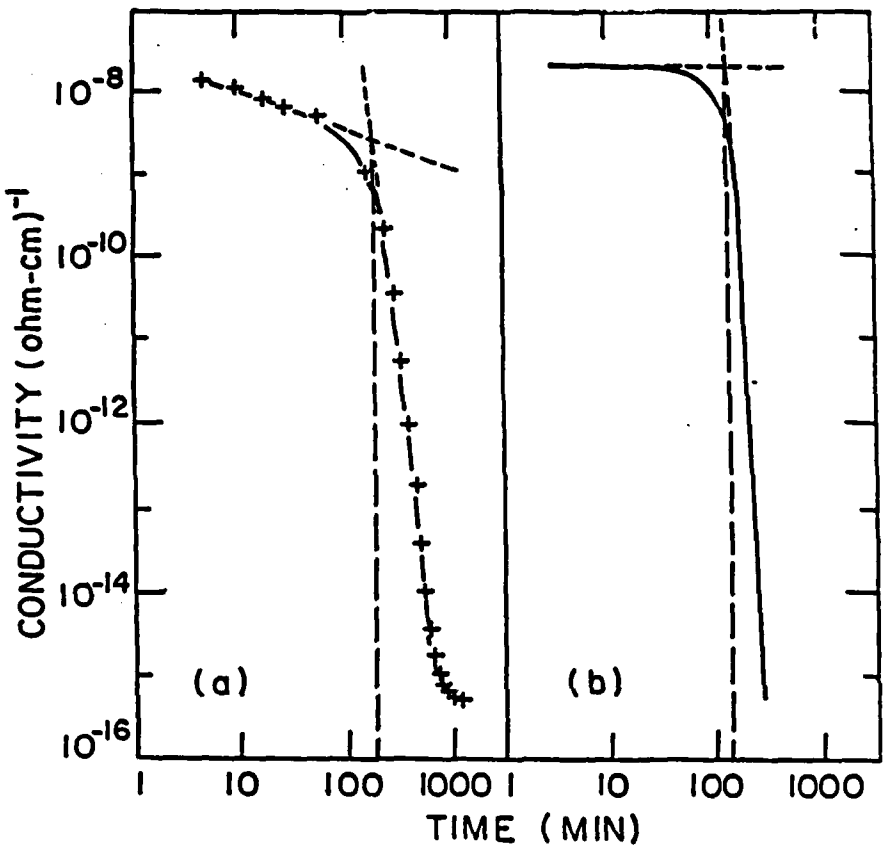

Figure 30 a) Conductivity data of Acitelli for the 57 °C cure of a low molecular weight DGEBA resin with m-phenylene diamine. (Reprinted from [60] with the permission of the publisher Butterworth Scientific, Ltd.). b) Simulation of the data of Figure 30a using a chemical kinetic model to determine T_g versus time and a WLF equation is to determine the conductivity. (Reprinted from [35] with permission of the Massachusetts Institute of Technology.)

DISTRIBUTION LIST

Dr. J. M. Augl
Naval Surface Weapon Center
White Oak, MD 20910

Prof. F. J. Boerio
Dept of Materials Science
U. of Cincinnati
Cincinnati, OH 45221

Prof. H. F. Brinson
Center for Adhesion Science
VPI&SU
Blacksburg, VA 24061

Dr. M. Broadhurst
National Bureau of Standards
Gaithersburg, MD 20899

Dr. Charles Browning
AFWAL/ML
WPAFB, OH 45433

Dr. Stan Brown
NADC
Warmenster, PA

Defense Technical Information Center
Cameron Station
Alexandria, VA 22314
(12 Copies)

Dr. Dawn Dominguez
Naval Research Laboratory
Washington, D.C. 20375

Dr. L. T. Drzal
AFWAL/MLBM
WPAFB, OH 45433

Prof. D. W. Dwight
Center for Adhesion Science
VPI&SU
Blacksburg, VA 24061

Dr. R. B. Fox
NRL Code 6120
Washington, D.C. 20375
Akron, OH 44304

Dr. Alan Gent
Institute of Polymer Science
University of Akron
Akron, OH 44304

Prof. Brian Hornbeck
U. S. Army R&D Center
STRBE-NBC
Ft. Belvoir, VA 22060

Dr. Don Hunston
Polymer Division
National Bureau of Standards
Gaithersburg, MD 20899

Prof. Wolfgang Knauss
Graduate Aeronautical Labs
California Technical
Pasadena, CA 91125

Dr. W. B. Moniz
Naval Research Laboratory
NODE 6120
Washington, DC 20375

Dr. L. H. Peebles, Jr.
Office of Naval Research
Code 431
800 N. Quincy St.
Arlington, VA 22217-5000
(2 copies)

Dr. R. R. Reeber
ARO
PO Box 12211
Research Triangle Park, NC 27709

Dr. Z. N. Sanjana
Westinghouse R&D Center
Pittsburgh, PA 15235

Prof. S. D. Senturia
MIT
Rm 13-3010
Canbridge, MA 02139

Dr. Robert Timme
NRL/USRD
Orlando, FL 32806

Dr. Ting
NRL/USRD
Orlando, FL 32806

Dr. Ron Trabocco
Code 60631
NADC
Warminster, PA

DISTRIBUTION LIST

Dr. J. D. Venables
Martin Marrietta Labs
Dept of Chemical Engineering
Princeton University, Wentworth
Princeton, N.J. 08540

Prof. T. C. Ward
Center for Adhesion Science
VPI&SU
Blacksburg, VA 24061

Dr. S. Wentworth
AMXMR-OP AMMRC
Watertown, MA 02172

Prof. J. P. Wightman
Center for Adhesion Science
VPI&SU
Blacksburg, VA 24061

Dr. Henry Wohltjen
Naval Research Laboratory
Code 6100
Washington, D.C. 20375

Dr. K. J. Wynne
Office of Naval Research
Code 413
800 N. Quincy St.
Arlington, VA 22217-5000

END

FILMED

11-85

DTIC